



**3D-PRINTED ADSORPTION MODULES FOR INDIUM RECOVERY FROM
SEAWATER BRINE**

Rahman Md Arifur

Lappeenranta–Lahti University of Technology LUT

Master's in Chemical Engineering and Water Treatment

2021

Examiner(s): Professor

Eveliina Repo, D.Sc. (Tech.)

Postdoctoral Researcher

Sanna Hokkanen

Abstract

Lappeenranta-Lahti University of Technology
LUT School of Engineering Science
Chemical Engineering and water treatment

Rahman Md Arifur

3D-PRINTED ADSORPTION MODULES FOR INDIUM RECOVERY FROM SEAWATER BRINE

Master's Thesis

2021

88 pages, 42 figures, and 5 tables

Examiners: Professor

Eveliina Repo, D.Sc. (Tech.)

Postdoctoral Researcher

Sanna Hokkanen,

Keywords: Indium; 3D printed TP260; Indium preconcentration; Seawater brine; Additive manufacturing; Column adsorption; Kinetic; Isotherm

Indium is a metal that is commonly utilized in the electronic industry. Consumption of Indium has increased dramatically, but supply has not kept pace with demand. Additionally, Indium is classified as a critical raw material due to the absence of large primary sources. Recycling Indium and recovering Indium from alternate sources is essential to meeting growing demand. Seawater brines were discovered to be a significant source of Indium, and technological development is required to recover it.

The purpose of this thesis was to develop a sustainable technique for Indium recovery from brine solutions. This research focuses on the recovery of Indium by adsorption technology using 3D printed adsorption modules. The effective adsorbent for In (III) adsorption was synthesized using additive manufacturing techniques. The 3D printed TP-260 adsorbent was utilized to preconcentrate In (III) using the column adsorption method and yielded 0.97 recovery of Indium.

By offering a larger surface area, a robust structure, facile separation from adsorbed solution, and simple recovery and regeneration by acid elution, additive manufacturing (3D printed technology) gave a significant advantage in the adsorption process.

Acknowledgement

I would want to appreciate and show my gratitude to my supervisor, Eveliina Repo, for providing me with an incredible opportunity to work with her research group on an innovative technology initiative. Her progressive encouragement, feedback, and friendly attitude (email with smiley 😊) inspire me to work fearlessly. I would like to express my gratitude to my research project partner Sea4value for the funding. I'd want to express my gratitude to my Lab supervisor Asiia Suerbaeva for her unwavering support throughout the research time. I could ask her any question and seek assistance without hesitation; her assistance with laboratory work, nice demeanor, and rapid response facilitated my research work. We would like to express our gratitude to Liisa Puro and Sanna Hokkanen for their assistance with the analysis effort (ICP, SEM, FTIR).

I would want to express my gratitude to my wife Papia Yasmin and my entire family for their unwavering support and understanding during my preparation of this thesis. Your prayers for me have kept me going this far.

Finally, I want to convey my thankfulness to Allah for allowing me to overcome all obstacles. Every day, I felt your guidance. You are the one who enabled me to complete my degree. I will continue to place my future in your hands.

Symbol and Abbreviations

Roman characters

p	pressure	[bar, Pa]
R	gas constant	[J/kg K]
T	temperature	[°C, K]
q_e	Equilibrium quantity of the adsorbate	[mg/g]
C_e	Equilibrium concentration of the adsorbate	[mg/L]
C_o	Initial concentration of the adsorbate	[mg/L]
K_L	Langmuir constant	[L/mg]
q_m	Maximum adsorption capacity	[mg/g]
K_F	Freundlich exponent	[mg/g]
n	Freundlich constant	
K_s	Sips isotherm model constant	[L/g]
K_a	Dissociation constant	[mol/L]
q_t	Quantity of adsorbent adsorbed at a time t	(mg / g)
K_1	First-order rate constant of adsorption	[1/min]
t	Time	min
K_2	Second-order rate constant of adsorption	[1/min ²]

Greek characters

α_s	Sips isotherm model constant	[L/g]
β_s	Sips isotherm exponent	

Abbreviations

AM	Additive Manufacturing
BJ	Binder Jetting
BET	Brunauer-Emmett-Teller
CAD	Computer Aided Design
CIJ	Continuous Inkjet
DED	Directed Energy Deposition
D2EHPA	Di-(2-ethylhexyl)phosphoric acid
EDS	Energy Dispersive X-Ray Spectroscopy
FTIR	Fourier Transform Infrared Spectroscopy
ICP	Inductive couple plasma
ITO	Indium Tin Oxide
IRA-743	Amberlite® 743
LCD	Liquid Crystal Display
MJ	Material Jetting
PSO	Pseudo-second-order model
PNP	Positive Negative Positive
PA12	Polyamide 12
PBF	Powder Bed Fusion
TBP	Tributyl Phosphate
TFT	Thin film Transistor
TP-207	Lewatit® TP-207
TP-260	Lewatit® TP-260

SEM	Scanning Electron Microscopy
STL	Standard Triangle Language
3D	Three-dimensional, or having three dimension

Table of Contents

Abstract.....	2
Acknowledgement	3
Symbol and Abbreviations.....	4
1. Introduction.....	13
1.1 Background	13
1.2 Objective of the research and contents.....	14
2. Indium.....	15
2.1 Source and production.....	15
2.2 Application of Indium resource.....	17
2.3 Supply and demand profile of Indium.....	18
3. Indium recovery techniques	20
3.1 Leaching	20
3.2 Pressure leaching.....	22
3.3 Extraction	23
3.4 Electrolysis	24
3.5 Cementation and precipitation	25
3.6 Extraction using sub-critical water.....	26
3.7 Extraction by supercritical fluid.....	27
3.8 Adsorption.....	27
4. Adsorbent materials for Indium recovery	30
4.1 Resin TP-207.....	30
4.2 Resin Lewatiti® TP-260	31
4.3 Amberlite® IRA-743	32
5. Additive Manufacturing.....	33
5.1 Powder Bed Fusion (PBF).....	34
5.2 Binder Jetting (BJ)	36
5.3 Directed Energy Deposition (DED)	37
5.4 Materials Extrusion (ME).....	37
5.5 Materials Jetting (MJ)	38
5.6 Sheet Lamination (SL)	39
5.7 Vat Polymerization (VP).....	40
6. Adsorption.....	41

6.1	Adsorption theory.....	41
6.2	Adsorption Isotherm.....	42
6.2.1	Basic isotherm category.....	42
6.2.2	Langmuir isotherm	44
6.2.3	Freundlich isotherm.....	46
6.2.4	Sips isotherm	46
6.3	Adsorption Kinetics.....	47
6.3.1	Pseudo first-order model	48
6.3.2	Pseudo second-order model.....	48
	The K_2 values is obtained from plotting tqt vs. t that called as rate constant.	49
6.3.3	49
6.3.4	Intraparticle diffusion model	49
6.4	Error Analysis	50
6.4.1	The sum of the square of the error (ERRSQ)	50
6.4.2	The hybrid functional error function (HYBRID)	51
6.4.3	The sum of absolute errors (EABS)	51
6.4.4	The average relative error (ARE)	51
6.4.5	Marquardt's percentage standard deviation (MPSD)	52
7.	Experimental Procedure.....	53
7.1	Materials and Methods	53
7.1.1	Reagents and chemicals.....	54
7.1.2	Additive manufacturing process	54
7.1.3	Preparation of Indium solution	55
7.1.4	pH dependency experiment	55
7.1.5	Batch adsorption procedure	56
7.1.6	Indium recovery from brine and regeneration.....	57
7.2	Adsorbent Characterization.....	58
7.2.1	Fourier Transform Infrared Spectroscopy (FTIR).....	58
7.2.2	Scanning Electron Microscopy.....	59
8.	Result and Discussion	60
8.1	Effect of pH.....	60
8.2	Effect of contact time	61
8.3	Kinetic analysis	62
8.3.1	Pseudo first order and pseudo second order kinetic model	63
8.4	Initial concentration effect	66

8.5 Adsorption Isotherms	68
8.5.1 Langmuir Isotherm	68
8.5.2 Freundlich Isotherm.....	70
8.6 Indium preconcentration and regeneration.....	71
8.7 Adsorbent characterization.....	72
8.7.1 Scanning Electron Microscopy.....	72
8.7.2 Fourier Transform Infrared Spectroscopy (FTIR) analysis.....	74
9. Conclusions.....	76
10. References.....	78

List of figures

Figure 1 The world production volume of Indium in China and whole world between 2007 and 2014.....	16
Figure 2 Indium global production rate	17
Figure 3 Main applications of Indium	18
Figure 4 Indium consumption and production forecast overview	18
Figure 5 Indium recovery from secondary sources globally	19
Figure 6 Standard flow chart Indium extraction from white ash.....	23
Figure 7 Illustration of simplified Indium recovery process by resin Lewatit® TP-207	30
Figure 8 Simplified diagram of TP-260 a) aminomethylphosphonic group with di sodium ions, b) aminomethylphosphonic group, c) illustrate Indium bonding site	31
Figure 9 Resin IRA-743 functional group molecular structure a) before adsorption b) after adsorption.....	32
Figure 10 3D model, b) STL format of 3D model c) slicing of 3D model	33
Figure 11 Steps of Additive Manufacturing	34
Figure 12 Illustration of Powder bed fusion technology	35
Figure 13 Illustration of Binder Jetting process.....	36
Figure 14 Two DED systems (A) utilize a laser and powder feedstock, whereas (B) use an electron beam and wire feedstock.....	37
Figure 15 Systematics diagram of Materials extrusion process	38
Figure 16 Systematic diagram of Material Jetting process (Sireesha <i>et al.</i> , 2018).....	39
Figure 17 Systematic diagram of Sheet Lamination.....	39
Figure 18 Systematic diagram for vat polymerization	40
Figure 19 Basic four isotherm type.....	43
Figure 20 Typical and 3D printed adsorbent	54
Figure 21 The Eh-pH diagram for Indium	55
Figure 22 Adsorption in batch mode	56
Figure 23 Indium recovery from brine and regeneration process.....	58
Figure 24 pH effect on In (III) adsorption by resin TP-207 at room temperature, 24h contact time and 500 rpm shaking speed.....	60
Figure 25 Final vs Initial pH of adsorbed solution	61

Figure 26 Effect of contact time on Indium adsorption process onto TP-207, TP-260, IRA-743 and 3D printed TP-260; temperature 25°C, shaking speed 500 rpm, initial concentration 150ppm for 3D TP-260 and other 50ppm initial concentration.....	62
Figure 27 In(III) adsorption pseudo first order and pseudo second order kinetic model for TP-207 adsorbent; 50ppm initial concentration, 500rpm shaking speed.....	63
Figure 28 In(III) adsorption pseudo first order and pseudo second order kinetic model for TP-260 adsorbent; 50ppm initial concentration, 500rpm shaking speed.....	64
Figure 29 In(III) adsorption pseudo first order and pseudo second order kinetic model for IRA-743 adsorbent; 50ppm initial concentration, 500rpm shaking speed.	64
Figure 30 In(III) adsorption pseudo first order and pseudo second order kinetic model for 3D TP-260 adsorbent; 50ppm initial concentration, 500rpm shaking speed.....	65
Figure 31 effect of initial concentration on In(III) adsorption by resin TP-207 at concentration range 5-200ppm, pH 3.5, contact time 12hr, shaking speed 500rpm and 25°C temperature...	66
Figure 32 effect of initial concentration on In(III) adsorption by resin TP-260 at concentration range 5-200ppm, pH 3.5, contact time 12hr, shaking speed 500rpm and 25°C temperature. .	66
Figure 33 effect of initial concentration on In(III) adsorption by resin IRA-743 at concentration range 5-200ppm, pH 3.5, contact time 12hr, shaking speed 500rpm and 25°C temperature.	67
Figure 34 effect of initial concentration on In(III) adsorption by 3D printed TP-260 adsorbent at concentration range 5-425ppm, pH 3.5, contact time 6hr, shaking speed 500rpm and 25°C temperature.	67
Figure 35 Langmuir isotherm model for TP-207, TP-260 and IRA-743 at concentration range 5-200ppm, pH 3.5, contact time 6hr, shaking speed 500rpm and 25°C temperatures.....	69
Figure 36 R_L vs concentration of In(III) plot.....	69
Figure 37 Freundlich isotherm model for TP-207, TP-260 and IRA-743 at concentration range 5-200ppm, pH 3.5, contact time 6hr, shaking speed 500rpm and 25°C temperatures...	70
Figure 38 SEM image of TP-207 before (left) and after adsorption (right)	72
Figure 39 SEM image of TP-260 before (left) and after adsorption (right)	73
Figure 40 SEM image of IRA-743 before (left) and after adsorption (right)	73
Figure 41 SEM image of 3D printed 3D TP-260 before (left) and after adsorption (right)	73
Figure 42 FTIR spectra TP-207, Nylon-12 and 3D TP-207	75

List of Table

Table 1 Seawater brine composition.....	57
Table 2 Pseudo first and pseudo second order kinetic model calculated parameter for In(III) adsorption with TP-207, TP-260 IRA-743 and 3D TP-260 adsorbent	65
Table 3 Langmuir and Freudlich isotherm model predicted parameter value	69
Table 4 Comparative study table	71
Table 5 In(III) preconcentration data	71

1. Introduction

This chapter discusses the history of research into Indium recovery using adsorption technology, includes an outline of the thesis's aim, and lists the thesis's relevant topics.

1.1 Background

Numerous electrical gadgets, the military, and a few other sectors make extensive use of Indium and Indium-based compounds, and the European Commission defines Indium as a critical strategic meta (Alguacil *et al.*, 2016). Researchers are concentrating their efforts on green energy to save fossil fuels and ensure the sustainability of the environment; solar energy is the primary source of green energy among others (Lahtinen *et al.*, 2017). The substantial performance of Indium-based compounds (copper Indium gallium selenide) in solar energy systems piques the researcher's interest—this project will soon require Indium (Sasaki, Oshima and Baba, 2017). However, the supply of Indium is limited due to the rarity of significant Indium-containing minerals. According to research, the amount of Indium found in nature as ore is extremely limited (4 to 10%); also, due to Indium's low recycling rate, its price has risen dramatically. To satisfy the growing demand for Indium and to ensure sustainability, manufacturing capacity must be expanded and recycling rates increased, as Indium ion has a carcinogenic impact that is damaging to the heart, kidneys, and liver.(Deferm *et al.*, 2017)

There are a few distinct techniques for recovering and recycling metals: Leaching, solvent extraction, ion exchange, electrolysis, cementation and precipitation, sub-critical water, and sub-critical fluid extraction (Pradhan, Panda and Sukla, 2017). Recent approaches, on the other hand, are not ecologically sustainable or cost-effective. The research discovered that the adsorption approach has the potential to overcome the prior technical barriers by providing more efficient selective recovery than other traditional methods.(F. Li *et al.*, 2018; M. Li *et al.*, 2018) Unfortunately, adsorption has a limited selectivity for Indium adsorption, necessitating additional adsorbent modifications.

Ion exchange resins are frequently utilized in the fabrication of a wide range of commercial resins, including Amberlite IRC748 and Lewatit TP-260, TP-207, and TP-208. Several adsorption investigations employing commercial resins for Indium recovery were conducted.

Recovery of Indium from the adsorbent using H₂SO₄/HCl elution yielded up to 99.5 percent Indium (M. C.B. Fortes, Martins and Benedetto, 2007; Jeon, Cha and Choi, 2015).

Over the last few decades, 3D printing processes and materials have been developed to create sophisticated mechanical structures utilizing resins, metals, and other compounds to include functional groups into the design. 3D printing is gaining popularity as a method for manufacturing ion exchange membranes, antimicrobial composites, and catalytically active materials. While the traditional adsorption technique utilizes a common adsorbent to adsorb metal ions, recycling the adsorbent and metal extraction from the adsorbent is not straightforward. On the other hand, 3D printed adsorbents do not require filtration because they are immersed in metal solution to absorb metals, and then Indium extraction and regeneration are done by simple elution. The purpose of this thesis is to develop an additively manufactured 3D printed adsorbent for the recovery of Indium from saltwater. The additive manufacturing process will be utilized to create 3D printed adsorbent. SEM, FTIR, BET, and XPS will be utilized to characterize the adsorbent, while ICP will be used to monitor the adsorption process.

1.2 Objective of the research and contents

The objective of this thesis was to design Indium selective an additively manufactured adsorbent using mixture of commercial resin and printing polymer.

To evaluate the efficient adsorption capacities of granular ion exchange materials and 3D printed resins, the following batch study was conducted at the LUT university laboratory: pH sensitivity test, batch isotherm, kinetics analysis, selectivity analysis, and regeneration analysis. ICP analysis was used to define the concentration of Indium. characterization of the adsorbent was conducted using FTIR for identifying the surface functional groups, SEM analysis to see the surface morphology, EDS for elemental analysis, and BET for measuring the surface area of the adsorbent.

A short theoretical overview reported in this work includes the Indium production, and demand, as well as Indium recovery routes and its various applications. Theories behind of conventional Indium recovery technologies, additive manufacturing, and adsorption methods are also discussed. Results and discussion section collects all the obtained data as well as interpretation and comparison of the results.

2. Indium

In 1863, Ferdinand Reich and Hieronymous Richter discovered Indium. They discovered it using spectroscopy; an indigo blue line formed throughout the experiment, indicating the presence of Indium. Indium was later referred to as Indium due to its origins in the indigo blue line (Haynes, W.M, Lide, 2010). Indium is a chemical element with the atomic number 49 and an electronic structure $[\text{Kr}] 4d^{10}5s^25p^1$. It is found in group 13, period 5, and block p of the periodic table. (Alfantazi, A.M.; Moskalyk, 2003) Indium appears silvery-white color that is a highly ductile post-transition metal having a bright luster. It is soft like sodium and has a lower melting point of 156.60 °C and a boiling point of 2072°C. Indium has a density of 7.31g/cm³, which is higher than that of gallium, and it acts as a superconductor at the critical temperature. (Haynes, W.M, Lide, 2010). The most common Indium ionization states are In(I) and In(III), where In(I) elements are referred to as strong reducing agents and Indium (III) elements have decreased stability and are no longer acting as oxidizing agents. (Greenwood, N.N.; Earnshaw, 1997)

In 1924, Indium was widely employed as a nonferrous metal (French, 1934). Indium was largely utilized as a coating material in high-performance aircraft bearings during World War II to avoid corrosion and wear-related damage, but this use is no longer frequently used in this industry (Greenwood, N.N.; Earnshaw, 1997). In the 1950s, a PNP transistor was constructed using a trace quantity of Indium. Indium phosphide and Indium tin oxide were developed as semiconducting materials for usage as thin film coatings in liquid crystal displays during the mid-1980s and late 1980s (LCDs). Thin film technique for those materials gained popularity in 1992 and is being utilized today across the world. (Downs, 1993)

2.1 Source and production

Indium does not have primary raw ore sources in earth's crust. It is retrieved as by product during processing of other metal's ore such as zinc sulfide and copper sulfide (Frenzel, Max; Mikolajczak, Claire; Reuter, Markus A.; Gutzmer, 2017). Indium compounds are transferred to the iron-rich residuals in the zinc refining processing plant. Depending on the extraction mode used in the smelter processing, different types of technologies are used to extract Indium from the residue and electrolysis is used as a final treatment technology for further purification

(Alfantazi, A.M.; Moskalyk, 2003) (Frenzel, Max; Mikolajczak, Claire; Reuter, Markus A.; Gutzmer, 2017).

The amount of Indium produced is proportional to the pace of zinc and copper sulfite production, since Indium is a byproduct of those ores, hence the phrase supply potential is used to describe the availability of Indium. The supply potential indicates the quantity of Indium that can be taken from mother resources in a given year based on current market conditions. According to the supply potential study, the existing Indium production capacity at the zinc sulfite and copper sulfite plants is expected to be 1300 tonnes/yr and 20 tonnes/yr, respectively. (Frenzel, Max; Tolosana-Delgado, Raimon; Gutzmer, 2015; Frenzel, Max; Mikolajczak, Claire; Reuter, Markus A.; Gutzmer, 2017).

According to the 2016 production report, China dominates the global market, producing approximately 290 tons of Indium, followed by South Korea, Japan, and Canada. Teck resource limited is another large company that operates an Indium production facility in Trail, British Columbia, with annual production volumes of 32.5, 41.8, and 36.1 tons in 2005, 2004, and 2003, respectively. (USGS, 2017)

Increasing the efficiency of Indium production and recycling may help to maintain the global market's demand-supply balance. However, the recycling rate is extremely low, less than 1%, and Japan is a leader in recycling of Indium.(USDI, 2011) Another source of Indium is seawater and wastewater, and an efficient Indium recovery technology can help to meet the increased demand. Figure 1 depicts the global Indium production scenario.

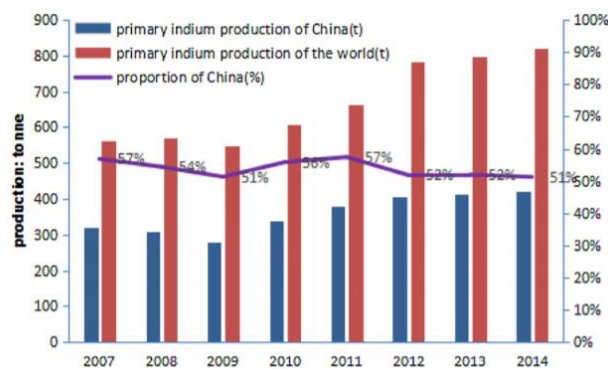


Figure 1 The world production volume of Indium in China and whole world between 2007 and 2014(data source: USGS).

Moreover, Figure 2 illustrates the global production of Indium from 1970 to 2020, with production began in 1970 and remained constant until 1985, after which the rate of production increased dramatically with time, and after 2000, the rate of production rocketed until 2020.

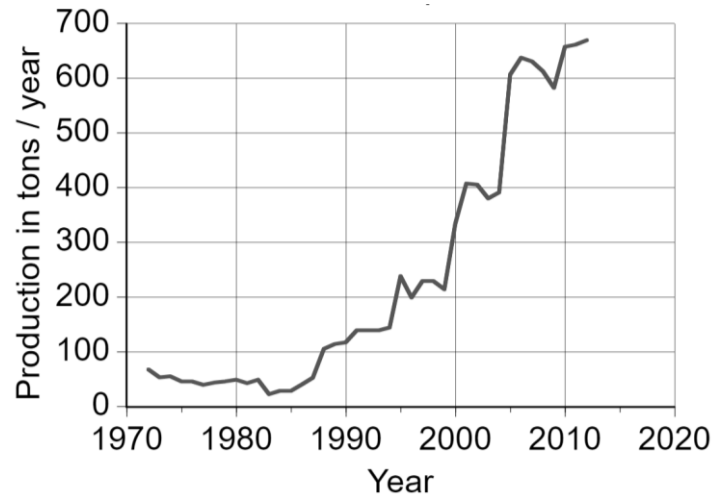


Figure 2 Indium global production rate (USGS, no date)

2.2 Application of Indium resource

Indium applications revolutionized the semiconductor industry by enabling the manufacture of electronic transistors, chip-like products, and a variety of electronic appliances, resulting in an increased demand for Indium. Indium oxide is heavily used in the manufacture of LCD screens, accounting for approximately 50% of total Indium production volume.(USGS, no date) The use of LCD screens has increased significantly as a component of computer and other electronic device screens such as mobile phones, cameras, and GPS receivers. Indium is used to construct electrical components in high-tech devices such as infrared detectors and photovoltaics. Due to its relatively low melting temperature, Indium is ideal for soldering and alloy production. Additionally, the use of ITO (Indium tin oxide) in the production of low-pressure sodium bulbs is very popular. Indium is widely used in the production of control rods in nuclear reactors, which produce neutron in the reaction process. Indium lymphocyte scintigraphy is used for nuclear medicine examinations to observe the characteristics of white blood cells. Furthermore, various forms of Indium like InSb, InP, InN are utilized in various fields, including light-emitting diodes, electroluminescent panels as coating materials, LEDs, as well as various semiconductor products.(Lokanc, Eggert and Redlinger, 2015) Figure 3 represents the main application of Indium.

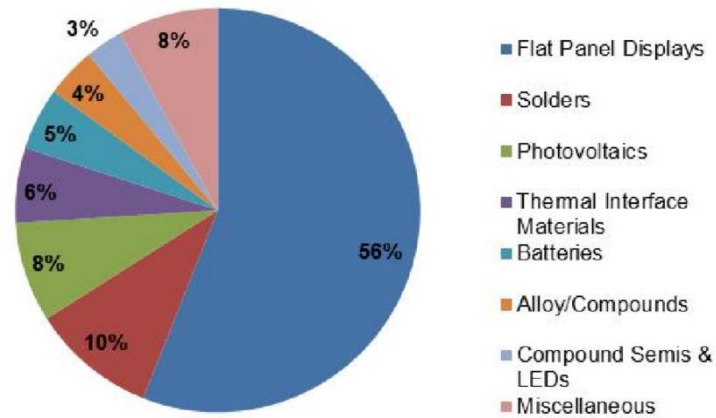


Figure 3 Main applications of Indium(Lokanc, Eggert and Redlinger, 2015)

2.3 Supply and demand profile of Indium

Indium supply is primarily dependent on zinc production, as Indium is a byproduct of zinc refinery plant. The area of Indium utilization is briefly described in Section 2.2, with the primary application being in the development of sophisticated electronic devices. The amount of Indium required to meet demand is 600-800 tons per year, and demand is increasing at a rate of 5% to 10% per year. Additionally, the increased demand for Indium in the electronic industry will put pressure on Indium supply in the future, as illustrated in Figure 4. According to the supply and demand profile, demand increases over time, but supply does not keep up with demand, resulting in a shortage of Indium in the year 2020. As a result, the price of Indium has been steadily increasing over the last few decades. (Hasegawa *et al.*, 2013)



Figure 4 Indium consumption and production forecast overview (Lokanc, Eggert and Redlinger, 2015)

To meet growing demand, researchers have concentrated on secondary sources such as recycling Indium products, seawater, and wastewater. Manufacturing waste and end-products are being used as a secondary source of Indium by countries such as China, Japan, and South Korea. Secondary sources include new scrap generated during the manufacturing process and used consumer products. However, due to the dissipative nature of old scrap, it does not recover significant amounts of Indium. (Li *et al.*, 2011) Figure 5 illustrates the global recovery of Indium from secondary resources, with Japan leading the way with the highest percentage of Indium recovered, followed by China, Belgium, and South Korea, while Canada and Germany recycle a nominal amount of Indium from secondary resources. (Lokanc, Eggert and Redlinger, 2015)

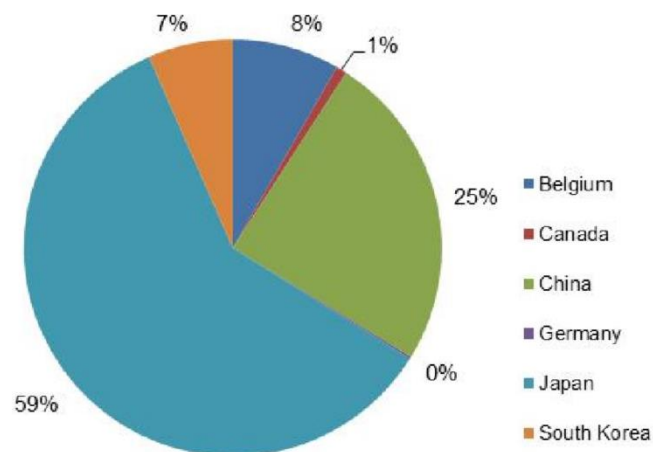


Figure 5 Indium recovery from secondary sources globally (Lokanc, Eggert and Redlinger, 2015)

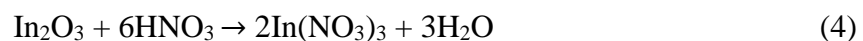
According to the (Amakawa, Alibo and Nozaki, 1996) study, the North Pacific Ocean contains 0.047-0.155 pmol/kg Indium, with prior research reporting Indium concentrations ranging from 26-52 pmol/kg in the eastern North Pacific as reported (Chow and Snyder, 1969) and 10-20 pmol/kg Indium in the North Atlantic as reported (MATTHEWS and RILEY, 1970). Seawater has been identified as an emerging secondary source of Indium. The purpose of this thesis is to develop technologies for recovering Indium from seawater brine that is generated at the desalination plant.

3. Indium recovery techniques

Indium's use in the development of electronic circuits has facilitated the advancement of computer, smartphone, and other electronic device usage. Thus, over 50% of Indium is consumed by the LCD screen manufacturing industries that degrades the global supply of Indium, as Indium is a byproduct of another manufacturing process. To address the vexing Indium crisis, it is necessary to recover from a secondary source. Currently, hydrometallurgical technologies, including leaching, electrochemical methods, extraction, and adsorption, depending on the production and quality, are used to recover Indium. The hydrometallurgical process for Indium recovery is advantageous due to its simple reaction control, common process parameters and operation control, low emission, and environmentally friendly nature. (Zhang and Xu, 2016)

3.1 Leaching

Leaching is one of the applications of hydrometallurgy, which is replacing pyro technology in the metal recovery field. Leaching is a mass transfer process that occurs at the solid-liquid interface when liquid substances react with the solid, primarily through oxidation and reduction reactions, extracting the target component into the liquid phase. Leaching agents, including acid, base, salt solution, and water, are vital components of the leaching process. (Petrucci, 2007) Indium dissolves in acid, forming the stable oxidation state In^{3+} , and the following reactions occur concurrently during the leaching process. (J et al., 2009; Ruan, Guo and Qiao, 2012; Silveira et al., 2015; Zhang and Xu, 2016)



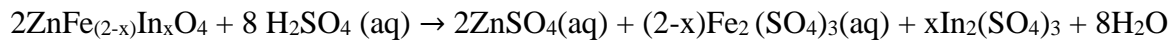
The dissociation rate of any metal in the leaching process is determined by the acid's dissociation constant (K_a). Because of its higher dissociation constant values, hydrochloric acid is suitable for any type of metal leaching, including Indium. (Li *et al.*, 2014a) Another

advantage of using HCl in the leaching process is that the end-product can be easily treated with NaOH to produce Sodium salt, which is non-toxic to nature.

Various studies have been conducted to recover Indium from various sources using a leaching process with various leaching agents. Vasiliki et al. conducted a study with various acid mixtures such as hydrochloric acid and water, hydrochloric acid, nitric acid, and water, and discovered that a water and hydrochloric acid mixture with a specific ratio ($H_2O:HCl=2:3$) had the highest leaching efficiency providing 60% Indium recovery (V, JN and E, 2015). Only Hydrochloric acid was used by Swain et al. to recover Indium and Tin from blended LCD screen in an oxidizing control chamber with maintained optimum concentration 5M, 500g/L ratio of solid to liquid, 348°K temperature, hydrogen peroxide 10%, speed of agitation 400 rpm and batch reaction time 2hr. (B et al., 2016a) Additionally, Fontana et al. recovered Indium from LCD screens over 90% without shredding or blending using concentrated 6M HCL. (D et al., 2015) Hot immersion technology, developed by Hsieh et al., is another efficient technique capable of achieving greater than 99 percent purity. In this operation, Indium-containing materials were immersed in a 30% HCl solution for 30 minutes to allow leaching. Then, at a temperature of 50 °C, pure magnesium and zinc were added to the solution to form an Indium sponge. This process is referred to as cementation precipitation and takes 30 minutes. Following that, the Indium sponge was converted to solid Indium using a hot immersion technique at a temperature of 300°C for 10 minutes. (Hsieh, Chen and Say, 2009) Another group of researchers, (Zhang et al., 2010), developed an Indium recovery method that uses less concentrated HCl (0.8M) in an ultrasonic environment and takes 60 minutes to complete leaching of a no-blend LCD screen. However, HCl leaching is only appropriate for secondary resources that include a small number of elements, such as LCD and ITO glass composed of Indium and Tin, which show no evidence of dissolution of primary sources. Additionally, although HCl leaching is not optimal for mineral resources with a low Indium concentration, its usage in leaching is beneficial since it does not need pretreatment prior to leaching, as other leaching agents such as H_2SO_4 do (Rocchetti et al., 2015). Because of the absence of a complex lixiviant process and the reusability of the system, the HCl leaching process usually involves counter current leaching containing several stages (B et al., 2016b). However, simultaneous organic discharge in solution from the LCD panel makes the recovery process harder, which is not beneficial (Rocchetti et al., 2015).

Sulfuric acid (H_2SO_4) became attractive in the hydrometallurgy sector due to its high proton donation capacity, suitability as a lixiviant, lower cost of manufacturing than other inorganic

acids, and ability to produce an ecologically acceptable end-product. Filippou and Demopoulos reported a skeletal reaction of Indium containing zinc ferrite and H_2SO_4 shown in eq (Filippou and Demopoulos, 1997).



The most often used method of dissolving metals in leaching is roasting with sulfuric acid at a higher temperature. Guocai et al. obtained more than 90% Indium from contained slag using an optimized system that included a controlled solid liquid ratio of 10%, a reaction duration of 1 h at 250 °C for roasting, a controlled solid liquid ratio of 10%, and a reaction time of 1 h at 60 °C for leaching (ZHU *et al.*, 2007).

Rocchetti et al. investigated a pathway for Indium recovery from LCDs using cross current leaching and the cementation technique. They used 2M H_2SO_4 to create an acidic environment and maintained an 80°C temperature for 10 minutes for ten sequential leaching operations followed by the cementation of sponge Indium recovery, which reduced greenhouse gas emissions. The ten-step leaching method significantly increases profit margins compared to the traditional one-step technique. (Rocchetti *et al.*, 2015)

3.2 Pressure leaching

Pressure leaching is a kind of leaching in which soluble minerals or concentrates are chemically dissolved under high pressure in order to extract the desired mineral from ores. Typically, this process is performed in closed autoclaves. Indium recovery is linked with zinc ferrite, which is found as a sulfide form in sphalerite, but the oxidation rate of sulfide is extremely slow under atmospheric oxygen pressure. (Crundwell, 1988) Pressure leaching is a method for dealing with the sluggish dissolving of In, Zn, and Fe. Li et al. performed a study for Indium and zinc recovery utilizing pressure leaching technique, obtaining 99 percent zinc and more than 90 percent Indium from sphalerite. The whole experiment was carried out in closed autoclaves in the presence of sulfuric acid and oxygen. To achieve maximum recovery, the process was optimized with particular particle size $48\mu\text{m}$, 1600 kPa oxygen partial pressure, 140 g/L sulfuric acid concentration, temperature of 160°C, and 150-minute operating time. (C. Li *et al.*, 2010) In another research, Indium was dissolved by pressure leaching from zinc oxide flue dust using sulfuric acid as a medium (X.-H. Li *et al.*, 2010).

A demonstration was carried out to determine the impact of oxygen pressure on the Indium leaching process, with the goal of increasing the oxidation rate in the leaching process. KMnO_4 (2.5 percent) and H_2O_2 (0.5mL/g) were employed in a sulfuric acid (5.1 M) environment with a temperature of 90°C and a reaction time control of up to 150 minutes to complete the leaching process and recover 90 percent of the Indium. Another research of leaching without oxygen pressure and without oxidizing agent achieved 77% Indium recovery, proving that oxygen pressure is not much advantageous for the Indium leaching process. (Pradhan, Panda and Sukla, 2017)

3.3 Extraction

In hydrometallurgy, extraction is referred to as solvent extraction, which is a more extensive kind of leaching for a few minerals processing. Due to the simplicity of the equipment design, the solvent's recyclability, and controlled process parameters, this method makes recovery feasible. Numerous studies have shown the solvent extraction process's viability for Indium recovery (Paiva, 2006) and Cyanex 923, bis-2, 2-ethylhexylphosphonic mono-2-ethylhexyl ester, and tributyl phosphate are the most often used extractants for Indium recovery. (Schaeffer, Grimes and Cheeseman, 2017)(Li *et al.*, 2014b). Yang *et al.*(Yang *et al.*, 2016) used Cyanex 923 and D2EHPA for Indium and yttrium extraction from white ash following standard flow chart of Guocai *et al.*(ZHU *et al.*, 2007) that is shown in Figure 6

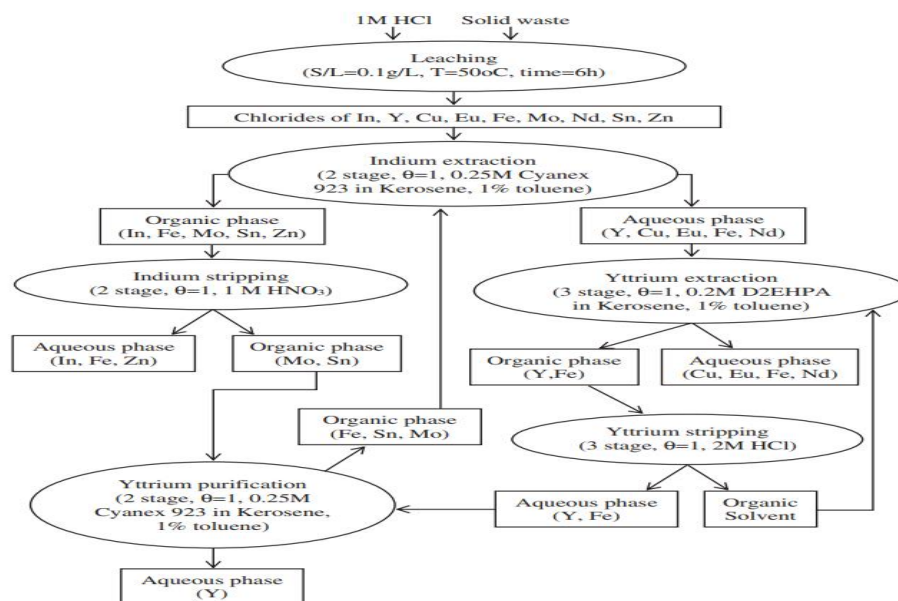


Figure 6 Standard flow chart Indium extraction from white ash (ZHU *et al.*, 2007)

In 2013, the same author investigated Indium selective solvents containing Cyanex 923, Cyanex 272, D2EHPA, and TBP. He discovered that diluted D2EHPA in kerosene provides high selectivity for Indium separation, exceeding 99 percent. Meanwhile, three solvent systems were investigated, including TBP, D2EHPA, and a mixture of the two, to recover Indium and Tin from LCD wastes. The mixture of TBP (0.8-1M) and D2EHPA (0.2M) separated Indium selectively from solution, whereas only the D2EHPA solution separated Indium and Tin simultaneously from solution. (Yang, Retegan and Ekberg, 2013) However, another research group showed that utilizing HCl stripping, Indium can be separated from the loaded D2EHPA. (Virolainen, Ibane and Paatero, 2011) Ruan et al. conducted a similar experiment utilizing three steps of processing with 97 percent separation, beginning with H₂SO₄ leaching, followed by D2EHPA extraction and lastly Indium recovery by HCl stripping. (Ruan, Guo and Qiao, 2012). (Chang *et al.*, 2016) demonstrated on a laboratory scale the separation of iron and Indium utilizing D2EHPA extractant from sulphate leach solution employing a steam rotating packed bed contractor and investigated effect of various parameters for instance extractant concentration, pH of initial solution, concentration of initial iron, ratio of flow rate and effect of gravity on the separation. Approximately 99% recovery was obtained using the following optimum parameters: 0.3 mol/L acid solution in feed, Aquas and organic flow ratio 2, organic phase flow rate of 30L/h, high gravity factor of about 83, extractant D2EHPA 25% vol in kerosene, 7g/L initial iron concentration, and 3mol/L HCl solution. Another research was performed in which Indium extracted using D2EHPA was recycled and utilized in a manufacturing facility through precipitation and calcination. (Chang *et al.*, 2016) Several studies have shown that D2EHPA extractant is superior for selective separation of Indium from various solutions using HCl as a stripping agent (Zhang *et al.*, 2017). Furthermore, Fontana et al. used polyethylene glycol to form a biphasic phase that yielded 80-95 percent Indium in the bottom extraction phase and 5-20 percent Indium in the top extraction phase (D *et al.*, 2015). Zonyl FSA was formed metal 1, 10-phenanthroline chelates complex during extraction and obtained 96.7% recovery of Indium (Kato *et al.*, 2013).

3.4 Electrolysis

Electrolysis is a method for separating desired products on the cathode or anode surface. Grimes demonstrated in 2017 the separation of Indium from Indium tin-lead-based compounds using electrolysis methods and leaching agents such as acetic and perchloric acid. In this work, a new cylindrical mesh electrode with three consecutive separation stages was utilized. Lead

was removed initially from the solution without the addition of the complexing reagent SCN^- , resulting in a recovery of 97 % of lead at a maximum concentration of 2 mg/L after an eight-hour reaction. The solution produced in the first stage is passed to the second step operation, which includes the addition of 0.02 mol/L complexing reagent SCN^- to aid in the multistep electrolysis process. The electrolysis procedure was performed for eight hours and recovered 94% of the tin at a concentration of 3mg/L. Finally, Indium was recovered as oxyhydroxide on the anode area and the concentration of SCN^- was increased to 1 mol/L to enable electrolysis. This electrolysis procedure took 24 hours and recovered 98% of the Indium (Grimes, Yasri and Chaudhary, 2017). Another study was conducted for Indium recovery from e -waste by utilizing HCl leaching process and extraction by PC88A extractant. To obtain maximum purity of Indium, electrolytic separating was used after extraction and 99.99% pure Indium was obtained. (Grimes, Yasri and Chaudhary, 2017)

3.5 Cementation and precipitation

Indium content is present in lead smelting dust in solid form; however, separation of Indium from dust is challenging owing to the existence of lead content in the dust; thus, lead content must be eliminated prior to leaching in order to extract Indium from lead dust. Sawai et al. developed a three-step processing method for recovering Indium from lead smelting dust. In the first stage, lead was separated using chelant aided washing with ethylene diamine disuccinate, which possesses selectivity for lead. For the leaching procedure, a solution of HCl and H_2SO_4 was employed, and dissolved Indium was recovered selectively by precipitation at pH 5, resulting in 88% recovery of Indium. (Sawai *et al.*, 2015). (Jiang, Liang and Zhong, 2011) conducted another research for Indium recovery from lead ore in which $\text{Na}_5\text{P}_3\text{O}_{10}$ was used to precipitate Indium in a pressured oxidation system. Under optimal conditions, the method demonstrated efficiency with 95 percent Indium recovery: molar ratio of $\text{Na}_5\text{P}_3\text{O}_{10}$ and Indium was 0.91, pH 2.6, and reaction time 1.5 hours. The precipitation produced as $\text{NaIn}_3(\text{P}_3\text{O}_{10})_2$ crystals, which was verified by XRD analysis, was then collected for further treatment, which started with dissolving the precipitate with H_2SO_4 for extraction. Later, at room temperature and pH 3.0, ZnO powder was added into the solution, which was maintained for 7 hours to complete the cementation process, yielding 97% pure Indium recovery. Another study utilized ammonia instead of $\text{Na}_5\text{P}_3\text{O}_{10}$ in a similar consecutive procedure that included precipitation, leaching, extraction, and cementation and 92% Indium recuperation from the 145 ppm Indium zinc plant waste was accomplished (Jiang, Liang and Zhong, 2011).

It is more appropriate to recover Indium from ITO wastes through an acid leaching and cementation process. However, the presence of tin in the leaching solution acts as a barrier to the cementation process, since it must be removed from the solution prior to the cementation process, which is a challenging procedure. (Li *et al.*, 2011) overcame the obstacle by introducing a sulfide precipitation into the process under optimal conditions, which included a 101.3Kpa H₂S partial pressure, a 100g/L H₂SO₄ concentration, a temperature of 60°C, and a precipitation duration of 10 minutes. Following that, zinc was added to aid in the development of the cementation sponge. Zinc concentration and cementation duration both have an impact on the purity of Indium. According to (Rocchetti, Amato and Beolchini, 2016) zinc concentration and duration are directly linked to cementation efficiency; as zinc concentration increases, Indium purity decreases, while increasing the time of the cementation process increases Indium purity.

3.6 Extraction using sub-critical water

Solvent extraction is used to aid Indium recovery during the leaching process in order to get pure Indium from the leaching solution. Separation of extractant solution after post treatment is challenging and requires additional recycling facilities, which is not ecologically favorable. Sub-critical water is an environmentally friendly technology that may be an ideal option for hydrometallurgical solvent extraction processes since it may overcome prior solvent extraction process limitations. Water characteristics vary as the temperature rises; the boiling point of water is 100 °C, and the critical point is 374 °C, at which significant pressure is required to maintain the liquid condition of the water, referred to as sub critical water. Water in the subcritical state decreases the dielectric constant, resulting in improved solubility for hydrophobic materials. Additionally, subcritical water increases the value of the ionic product by thrice at 250 °C compared to ambient temperature.(Tavakoli and Yoshida, 2006) Sub-critical water has been used in several works to recover different products from wastes such as amino acid, fatty acid, organic acid and nutrients (H, M and Y, 1999; Tavakoli and Yoshida*, 2005). Using sub-critical water and a five-minute reaction period, Indium was recovered from color filters and thin-film transistors at rates of more than 83% and 7%, respectively. The major benefit of this method was that Indium was separated from waste as Indium oxide in solid form, which can be readily separated from liquid solution, and the separation efficiency is influenced by sub-critical water temperature.(Yoshida *et al.*, 2014) investigated the impact of various basic chemicals present in separation systems, such as potassium hydroxide, sodium hydroxide,

ammonia, sodium carbonate, calcium hydroxide, and diethyl amin, as well as their concentration, on Indium recovery. With the same reaction time and temperature at 160°C, 0.1 N NaOH recovered over 95% of the Indium from TFT glass and 99% from color filter glass (Yoshida *et al.*, 2015). While the method offers several advantages for Indium recovery, it requires a significant amount of energy and money to construct the infrastructure necessary to maintain high pressure.

3.7 Extraction by supercritical fluid

Supercritical fluid extraction is superior to conventional fluid extraction because it is a green technology that achieves higher separation rates and efficiencies while using nontoxic, low-cost, and nonflammable liquefied CO₂. Additionally, it is more eco-friendly than traditional fluid extraction.(Ghoreishi, Ansari and Ghaziaskar, 2012) CO₂-based supercritical fluids reach supercritical phase at or above the critical temperature (31.1°C) and pressure (7.38MPa) with the same density as liquid CO₂. Viscosity is reduced compared to CO₂ and high solubility capacities are observed due to huge diffusion capabilities, lower viscosity, and zero surface tension.(Ghoreishi, Ansari and Ghaziaskar, 2012) A study discovered that supercritical fluid extracts Indium (76.5%) directly from ITO and cellphones using co-solvents such as citric acid and malic acid at ambient pressure and that the process took 180 minutes to complete. While only supercritical CO₂ achieves remarkable separation (94.6 percent recovery) in a short period of time and without the use of a co-solvent (30 min).(Argenta *et al.*, 2017)

3.8 Adsorption

The Indium recovery technologies discussed previously have limitations in several areas, including the fact that leaching is not always sufficient for Indium recovery; additional technologies such as solvent extraction, precipitation, electrolysis, and cementation are required to recover Indium from leaching solutions. Following processing, leaching and solvent extraction produce a large quantity of hazardous chemicals that drain into the environment, which is not environmentally friendly. Those processes take much more time than the production volume and product quality in terms of purity. In terms of mechanism and process control, the process is complicated and difficult to comprehend. In contrast, the adsorption method for Indium recovery is most flexible in terms of selectivity, simplicity and environmental friendliness.

Several adsorption studies were carried out utilizing commercial resin for Indium recovery to reveal adsorption properties and determine operating parameters in a thorough way (Jeon, Cha and Choi, 2015). Due to its selectivity, ease of functionalization, and ease of extraction of Indium from adsorbent, ion exchange resins became an appealing subject for Indium recovery. Iminodiacetic acid-based resin is commonly utilized in the manufacture of a variety of commercial resins, including Amberlite IRC748, Lewatit TP-260, and Lewatit TP-207. Fortes et al. investigated the capture of Indium on the commercial resin Amberlite IRC748 using dynamic adsorption and obtained 99.5% Indium recovery using H_2SO_4 elution at a flow rate of 5.0 mL/min (M. C. B. Fortes, Martins and Benedetto, 2007). Using iminodiacetic acid resin, (XIONG and YAO, 2008a) investigated the impact of various parameters on Indium adsorption and determined the parameter values for maximum adsorption of 235.5 mg/g at 25°C temperature and pH 4.52. (Yuchi *et al.*, 1992) did another investigation to evaluate the adsorption equilibrium of various metal trivalent ions (M^{3+}) utilizing chelating resin incorporating iminodiacetic acid. This study demonstrated the impact of anions and iminodiacetic acid ratio on formation of metal ligand complex for adsorption and determined the amount of iminodiacetic acid groups per unit weight. Few research has been made for metal adsorption e.g. In, Eu, Cu, Co, Ga, Ni using chitosan which is natural modified polymeric substances.

Assefi et al. investigated the recovery of Indium from waste LCD panels using three distinct microporous ion exchange resins (Lewatit TP-208, Lewatit TP-260 and Amberlite IRA 743). TP-208, for example, is made of iminodiacetic acid resin and has been demonstrated to be a better ion exchange for Indium recovery. Indium recovery is dependent on a number of variables, including pH, solute concentration, and temperature. In this investigation, pH values ranging from 0.5 to 4 were used to determine Indium recovery. At lower pH values, such as (pH 1-2), Indium ion generates hydronium ion, which acts as an inert towards adsorbent sites. As pH values increase, Indium recovery increases until pH 4. Above pH 4, the Indium ion generates $In(OH)_3$, a phase that has difficulties adhering to the adsorbent surface. By eluding Indium from resin with HCl acid, Indium was recovered. (Assefi *et al.*, 2018a) Another study was done on Indium recovery utilizing TP-207 to determine the Indium adsorption behavior and revealed a 55mg/g adsorption capacity at pH 0.8 (Lee and Lee, 2016) and the technique for recovering Indium from resin was identical to that described in a previously published work. (Assefi *et al.*, 2018a) Ferella et al. investigated the Indium recovery method using commercial

Amberlite IRA-748 and got the highest adsorption capacity at pH 3 with a 24hr contact period. (F *et al.*, 2017)

Due to the rarity of specific Indium adsorbent materials, numerous studies have been undertaken on functionalizing resins for selective Indium adsorption. Chang *et al.* developed chelate fiber resin for selective adsorption and obtained 95% recovery from a mixture of Sn, Cr, Ti, and In at pH of 4-7 with a feed flow rate of 10mL/min. (X *et al.*, 1993) (Yuan *et al.*, 2010) studied the coated solvent impregnated resin for selective Indium recovery and determined that the optimal pH for Indium adsorption was 1.5. Additionally, (Li *et al.*, 2012) modified a coated solvent impregnated resin with a styrene-divinylbenzene copolymer supported sec-octyl phenoxy acetic acid. This offered Indium selectivity at pH 3 across a wide temperature range and was stable for three successive regenerations. The Indium adsorption process was investigated using multiwalled carbon nanotubes, which had an adsorption capacity of 40 mg/g. However, the disadvantage of this adsorbent was that it was not selective when other metal ions were present in the solution. (Akama, Suzuki and Monobe, 2016)

Since the previous several decades, additive manufacturing has gained popularity for a variety of applications, including industrial, water treatment, and environmental concerns. The use of raw materials and the application of additive manufacturing technologies are increasing dramatically as they are used in the emergence of new technologies with success and application. This technique is associated with various instruments, which enables layer-by-layer deposition to obtain the required mechanical and chemical qualities.

The technique requires less material, which lowers the cost of production. (Gibson, Rosen and Stucker, 2010) Recently additive manufacturing technologies has been used for adsorption and ion exchange membranes for selective metal recovery. Lahtinen *et al.* developed an additively manufactured adsorbent for gold recovery using nylon-based materials. This results in a greater recovery % because nylon 6.6 and nylon 12 have a stronger affinity for gold while AM-based adsorbents have a larger surface area and mechanical stability, which increases the adsorbent's reusability.(Lahtinen *et al.*, 2019) Another study was made for selectively recover metal such as Pd, Pt, Au from e-waste using 3D printed scavenger filter. A mixture of polypropylene and anion exchanger resin was used to produce adsorbent that especially abled to capture Pd and Pt from waste. (Lahtinen *et al.*, 2018) This principle is used in this thesis work for manufacturing 3D printed adsorbent for Indium recovery from sea water.

4. Adsorbent materials for Indium recovery

Numerous studies on Indium recovery have been conducted using a variety of adsorbent materials, including ion exchange resins,(M. C. B. Fortes, Martins and Benedetto, 2007) chelating cellulose,(Akama, Suzuki and Monobe, 2016) modified metosol reagent,(Timofeev *et al.*, 2017) chelating fiber, microbeads, and carbon nanotubes. Three distinct adsorbent materials (Lewatit® TP-207, Lewatit® TP-260, and Amberlite® IRA-743) were used in this thesis to produce additively manufactured adsorbents, and their effectiveness was evaluated and compared. This section gives an overview of those materials.

4.1 Resin TP-207

Lewatit® TP-207 is a commercial cation exchange resin that is produced using an iminodiacetic acid-based chelating agent. It is designed specifically for the adsorption of heavy metals from solution. This is a mildly acidic material that is capable of functioning in weakly acidic or basic solutions.

Lewatit® TP-207 Indium recovery process is depicted in Figure 7 Resin Lewatit® TP-207 is composed of iminodiacetic acid in its sodium form, where the iminodiacetic acid group contains hydrogen or sodium ion, which acts as an ion exchanger. These mobile ions are replaced by Indium ions during the adsorption phase, and chelating occurs as well. (M. C. B. Fortes, Martins and Benedetto, 2007; XIONG and YAO, 2008b)

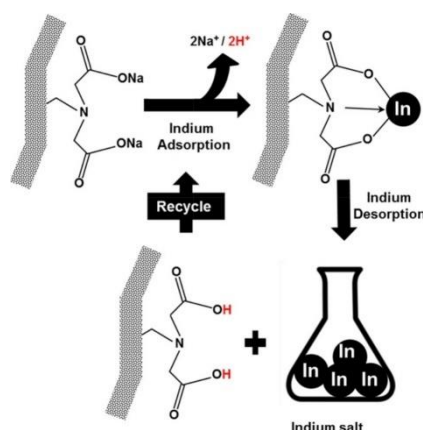


Figure 7 Illustration of simplified Indium recovery process by resin Lewatit® TP-207 (Lee and Lee, 2016)

After the adsorption process is complete, the adsorbent is filtered from the solution and the resin is transferred to an acid solution for desorption. By introducing a hydrogen ion to the resin, Indium can be removed. This hydrogen ion continues the adsorption process in the same manner as the preceding adsorption phase. TP-207's Indium recovery procedure is extremely easy and convenient in comparison to other approaches. The adsorption capacity of this resin is dependent on few operational parameters, including pH, temperature, and the concentration of various metal ions presence in solution.(Lee and Lee, 2016)

4.2 Resin Lewatiti® TP-260

Lewatiti® TP-260 is a cation exchange resin composed of an amino methyl phosphonic acid group that demonstrates selectivity for heavy metals and is naturally mildly acidic. The resin is microporous and contains disodium ions that attract metal ions from solution via ion exchange and the production of chelates with the metal ion. (Lewatit-Lenntech, no date) A study have established that phosphonic acid has an affinity for the Indium ion.(Assefi *et al.*, 2018a)

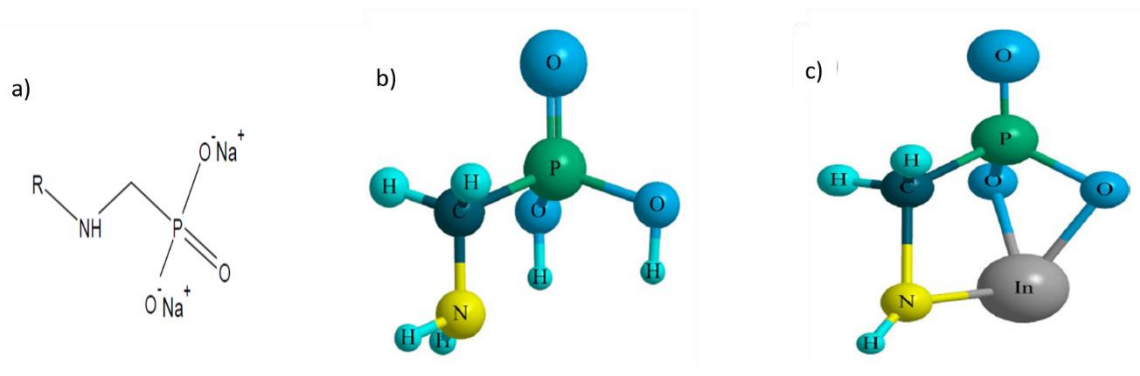


Figure 8 Simplified diagram of TP-260 a) aminomethylphosphonic group with di sodium ions, b) aminomethylphosphonic group, c) illustrate Indium bonding site (Source: adapted from (Kaukinen, Sc and Virolainen, no date) & (Assefi *et al.*, 2018a))

TP-260 has three active sites for the formation of ligands, including a phosphonic acid group that forms bonds, a nitrogen atom that acts as a coordinating site, and a disodium ion that undergoes ion exchange.(Kaukinen, Sc and Virolainen, no date) The Figure 8 depict the Indium adsorption site and the Indium adsorption site under mild acidic conditions. Indium adsorption happens in the following manner. When TP-260 fresh resin is used for adsorption, the resin contains sodium ions that are involved in Indium adsorption and recovery. Acid solutions are

often employed for Indium recovery and resin regeneration, with hydrogen ions occupying the resin. Later, the hydrogen ion serves as an ion exchange site for the recovery of Indium.(Assefi *et al.*, 2018a) In this thesis, disodium-based TP-260 resin powder was utilized resin for additive manufacturing.

4.3 Amberlite® IRA-743

Amberlite® IRA-743 resin is a weakly basic material composed of an N-methylglucaomine group with the ability to adsorb Indium from solution, as demonstrated in research. Although this material has a lower adsorption capability than the previously listed adsorbent materials. (Assefi *et al.*, 2018a)

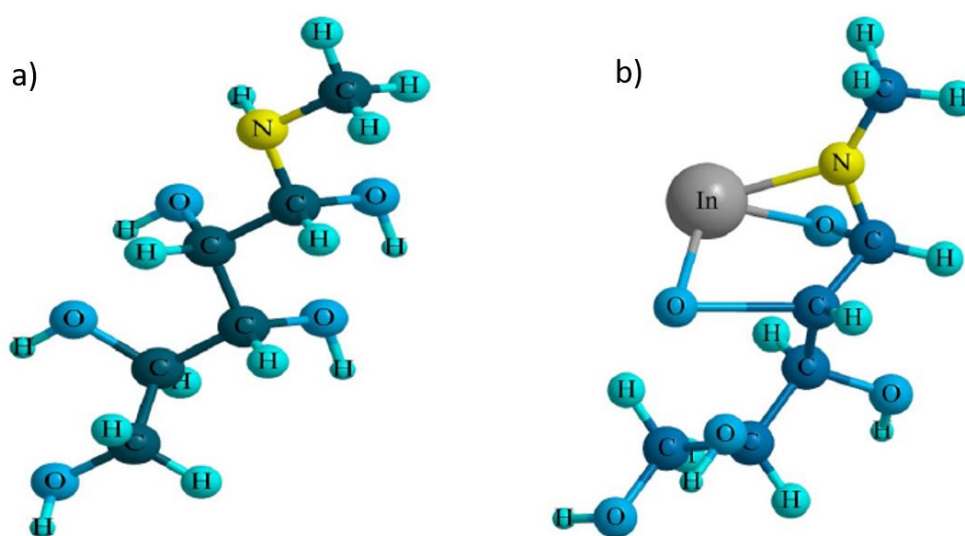


Figure 9 Resin IRA-743 functional group molecular structure a) before adsorption b) after adsorption (Assefi *et al.*, 2018a)

The Figure 9 depicted the molecular structure of the functional group, highlighting the active site when feasible by creating a bond with metal. The adsorption occurs by substituting hydrogen by Indium in N-methylglucaomine. The Indium is recovered from the resin using acid elution procedures that both recover the Indium and regenerate the resin.

5. Additive Manufacturing

According to the Oxford definition, a process is a sequence of activities or steps taken to obtain a desired outcome. Additive manufacturing (AM) is a set of operations that involve material selection, material assembly methods, and the conversion of raw materials to three-dimensional objects. Additive manufacturing works by layering and assembling to create the final envisioned structure. A Computer Aided Design (CAD) program (or other similar software) is used to create a three-dimensional model of the required design. The resulting model is not sliced as indicated in the Figure 10

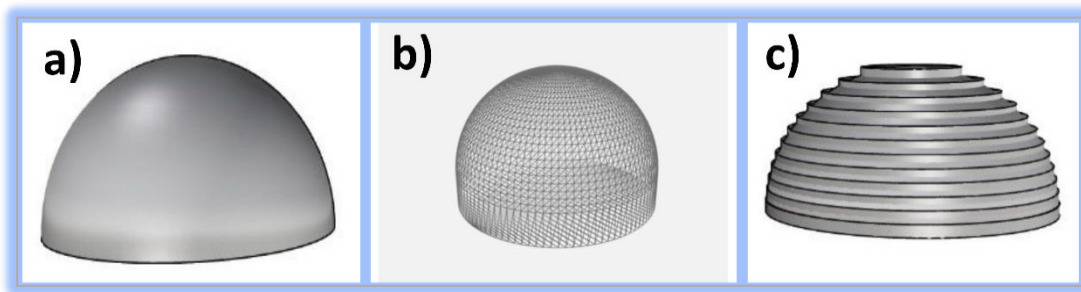


Figure 10 3D model, b) STL format of 3D model c) slicing of 3D model (Understand and fix common STL file errors | Hubs, no date; Ren and Galjaard, 2015)

Several considerations should be made during product design, such as lattice design and topology optimization, to guarantee minimal material consumption and high-quality goods. Prior to transferring the 3D model to the slicer software, it must be converted to the STL (Standard Triangle Language) format, which breaks the 3D model down into many tiny, linked triangles. When the boundary is curved, the triangle will not fit the model's boundaries, resulting in a gap between the boundary lines. Later, the STL model is transferred to a slicer application, which intersects the 3D model horizontally at several points according to the specified thickness value and stores the data for those coordinates, with the distance between two consecutive intersecting points being identified as the layer thickness. (Roschli *et al.*, 2019) The slicer program generates data and saves it to the computer in the form of G-code which maps the route taken by the printing equipment while creating the physical layer from virtual data. The lowest layer is created initially, and the printing procedure is repeated until the topmost layer is reached sequentially. A layout of successive action required for AM is shown in Figure 11



Figure 11 Steps of Additive Manufacturing (Kumar, 2020)

Every printing machine uses the same 3D CAD model and generated G code, but technologies are divided into seven groups depending on how they operate, such as powder bed fusion, binder jetting, Directed Energy Deposition, materials extrusion, materials jetting, sheet lamination, and vat polymerization (Deckers, Vleugels and Kruth, 2014). The advantages of additively manufactured adsorbents (3D printed adsorbents) are their mechanical stability and optimized structure for the adsorption process. Separation of adsorbent following adsorption is easier than conventional filtering, since it may be accomplished without the need of filter paper or membrane.

5.1 Powder Bed Fusion (PBF)

Powder bed fusion is a potential additive manufacturing technique for plastic materials, and it may be used at any scale from small to large. The most typical components found in a PBF printer are fiber lenses, scanning mirrors, laser beams, building platforms, powder dispenser platforms, recoater blades, and pistons for powder dispense, as illustrated in Figure 12. The PBF principle of operation is as follows: The printing process begins with preheating the polymer powder near its melting point, then distributing the heated polymer powder evenly on the building platform according to layer thickness with the help of a recoater blade that moves from right to left. Afterwards, scanning with a CO₂ laser beam on the construction platform begins in order to sinter the polymer powder that forms the structure's single cross section layer. After scanning each cross section of the building platform, move down one step according to layer height and spread powder on the building platform as before, continuing until the object's construction is complete. The scanner's scanning instructions and other commands, such as layer thickness and structural coordination, are read from the G-code sent to the printer. 3D objects must be ejected from the construction platform at the conclusion of the procedure, and unsintered powder must be removed from the item. PBF technique does not need a supporting framework since powder materials serve as the 3D object's supporting structure. The remaining powder may be utilized for future printing projects, and fresh powder should be mixed with old powder in a 1:1 ratio. (Ben Redwood and Filemon Schöffner, 2017)

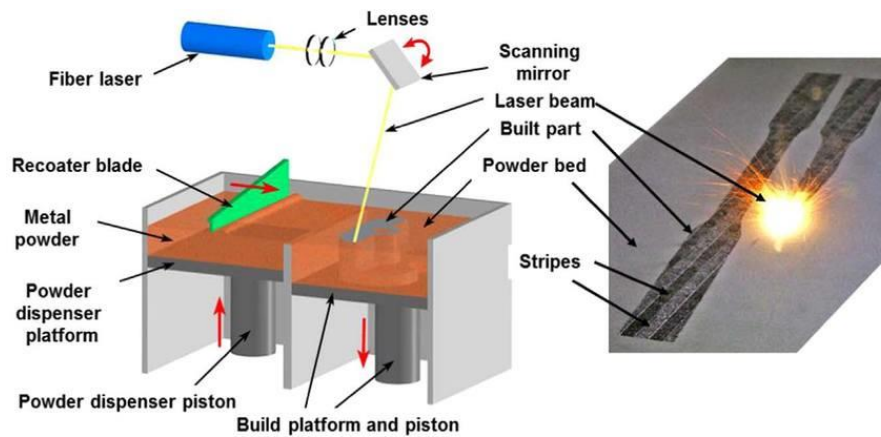


Figure 12 Illustration of Powder bed fusion technology (Criaies *et al.*, 2017)

Several factors must be considered throughout the PFB process since material characteristics and printing settings have an impact on the end product's quality. The mechanical characteristics of finished 3D structures are directly affected by material parameters such as powder particle shape and size, crystallinity, and molecular weight of polymer. The molecular weight and crystallinity of a substance affect its tensile strength and elongation, whereas grain size distribution affects powder fusion ability. (Hofland, Baran and Wismeijer, 2017)

The quality of 3D objects is also affected by printing machine parameters such as laser power, scanning speed, energy density, laser spot size, and layer thickness. The change in energy density is proportional to the change in laser power, which is responsible for polymer fusion. As the laser power increases, the energy density increases proportionally, leading to higher polymer fusion. Excess energy density destroys the polymer, while low energy density leads to incomplete melting of polymer powder, which affects the final product's tensile strength and elongation. (Ho, Gibson and Cheung, 1999) The fusing of polymer is affected by laser scanning speed and laser power, with lower laser speeds resulting in porous (diameter >100 m) structures and higher laser speeds resulting in dense structures. (Caulfield, McHugh and Lohfeld, 2007)

Because of its availability and mechanical characteristics, polyamide 12 (PA12) is a commonly utilized material in PBF printing. The product quality may be altered by combining various elements, including as carbon, aluminum, glass, and others, according to the requirements. This printing method reduces powder waste since it may be used many times with fresh powder and the leftover powder can sometimes be utilized to make filament for the filament printing process. (Feng, Wang and Wei, 2019)

This printing technique was utilized to manufacture 3D adsorbent for metal recovery in this thesis study. Various kinds of ion exchange resins were utilized in combination with polymers such as PA12 and nylon to manufacture 3D adsorbents for Indium recovery.

5.2 Binder Jetting (BJ)

Binder jetting is an additive manufacturing technique that uses a liquid binder to selectively bond powdered materials for the creation of 3DP objects rather than heat. Powder reservoir, liquid binder reservoir, print head inkjet, roller, powder bed, and building platform are all typical components of binder jetting printers shown in Figure 13. The printing process is broken down into the following steps: By roller, powdered materials are distributed evenly on the building platform, and then the printer head injects adhesive into the materials atop where needed. Finally, the building platform is stepped down, as in PBF technologies, and fresh powder is distributed on the building platform as before. The same technique is followed until the printing process is completed. Ceramic as powder and various kinds of binders, such as silicate, aqueous binder, phenolic, and furan, are typical materials used in this procedure. (Sachs *et al.*, 1993) This technique is divided into two kinds depending on the materials used in the printing process: printing with dry powder agglomerates and slurry-based 3D printing. Printing with dry powder is the same as described in this section, however, printing with slurry-based materials necessitates the use of extra heat to evaporate the liquid and produce powder for the printing process. (Deckers, Vleugels and Kruth, 2014)

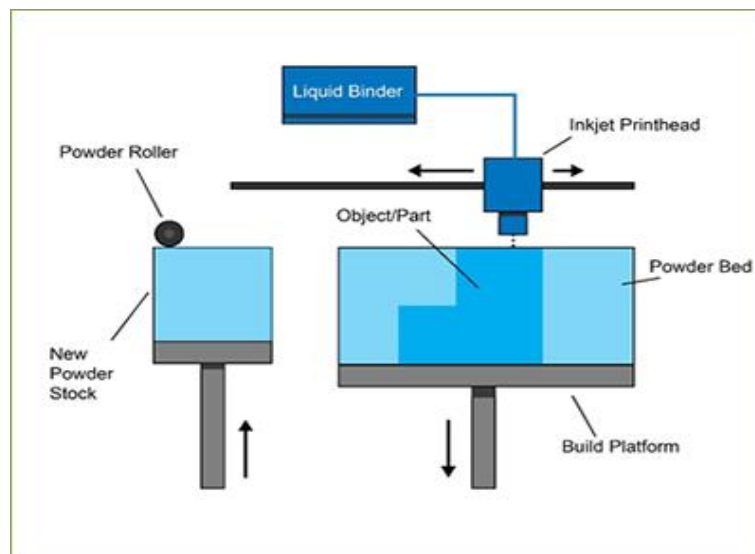


Figure 13 Illustration of Binder Jetting process (*Binder Jetting | Additive Manufacturing Research Group | Loughborough University, no date*)

5.3 Directed Energy Deposition (DED)

The directed energy deposition technique works by melting materials with thermal energy, then depositing the molten materials on a construction platform and solidifying them with a cold surface. This technique is classified into two kinds depending on the energy supply to the system: directed energy deposition, also known as laser cladding in certain contexts, which is a classic approach. This technology comprises of a laser beam and a nozzle that melts powder material and deposits it layer by layer on the substrate according to the item design. (Balla, Bose and Bandyopadhyay, 2008)

The use of hybrid fused deposition modeling developed by the University of Birmingham improved energy deposition to the system. In this method, hybrid technology was used, such as the use of an electron beam instead of a laser beam feed connected via wire made of Ti-6Al-4V that was directed to the beam rather than the nozzle (Wang *et al.*, 2007) shown in Figure 14.

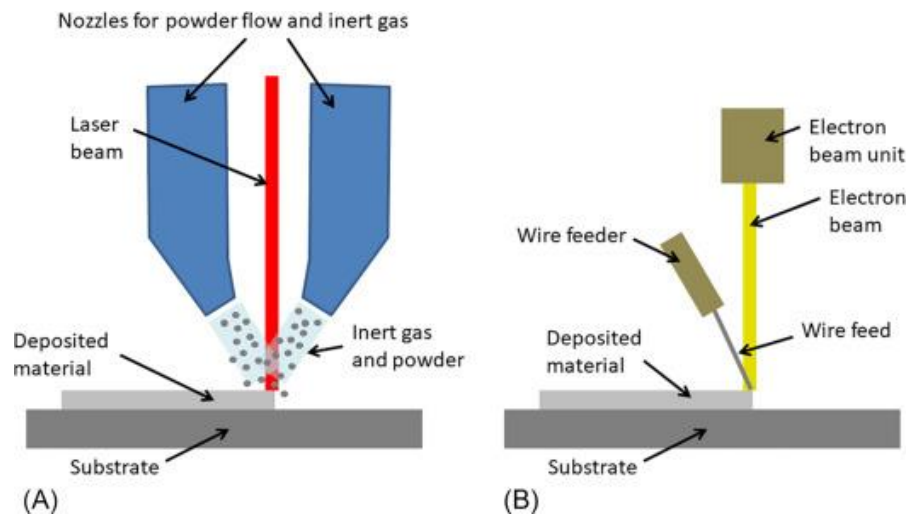


Figure 14 Two DED systems (A) utilize a laser and powder feedstock, whereas (B) use an electron beam and wire feedstock. Source: (Sing *et al.*, 2020)

5.4 Materials Extrusion (ME)

In materials extrusion techniques filament for printing process is taken to the heating zone where it melts and dispenses by the nozzle or orifice and deposits on the building surface layer by layer, this process requires supporting element during printing process. Following the first cross section layer second layer deposits on the top of that and fuses together as they are in

melted state. This process requires minimal materials and low cost for additive manufacturing shown in Figure 15. (Deckers, Vleugels and Kruth, 2014)

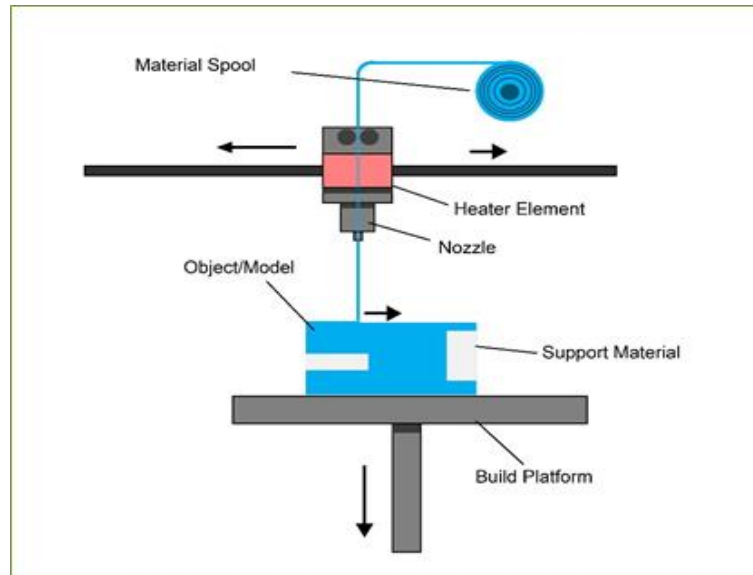


Figure 15 Systematics diagram of Materials extrusion process Source: (*Material Extrusion / Additive Manufacturing Research Group / Loughborough University, no date*)

5.5 Materials Jetting (MJ)

Materials jetting technology creates droplets of construction materials that are placed layer by layer on a building platform and immediately cured by UV light shown in Figure 16. Inject printing and Aerosol jet printing are the two kinds of this technique. Build materials comprising suspension are directly applied to substrate selectively by droplet in inkjet printing technique. The droplet goes through a phase transition and becomes a solid structure. While building ingredients spray on the building substrate in gas phase in aerosol jet printing, the quality of the product is smoothed because tiny particles are used instead of droplets. (Deckers, Vleugels and Kruth, 2014)

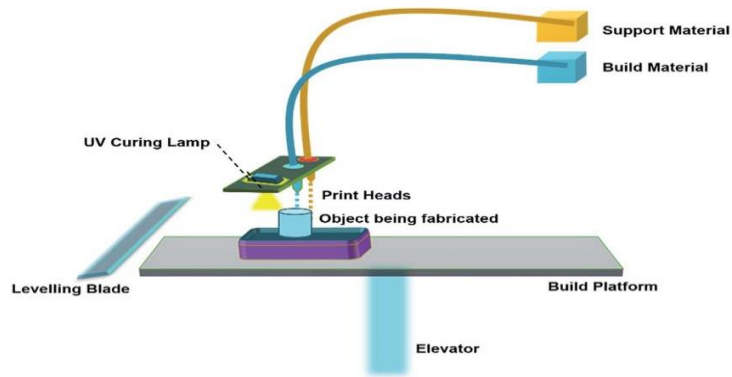


Figure 16 Systematic diagram of Material Jetting process (Sireesha *et al.*, 2018)

5.6 Sheet Lamination (SL)

Sheet lamination is a technique that involves gluing sheet materials together for additive manufacturing. It is sometimes referred to as laminated object modeling (LOM). This procedure is divided into two categories according to its operating principle. Using brazing, bonding, or welding, sheets are joined together to create an object. For the printing process, sheet materials are put on the cutting bed for subsequent bonding. Depending on the shape of the product, more materials are cut from the bonded sheet using a laser or a knife. This technique evolves and includes computer-assisted cutting, with each layer being cut robotically prior to lamination. An illustration of sheet lamination process is shown in Figure 17. This technique is inefficient for precise designed objects and generates a significant quantity of trash. However, the materials cost of this method is low, which contributes to its appeal. (Deckers, Vleugels and Kruth, 2014)

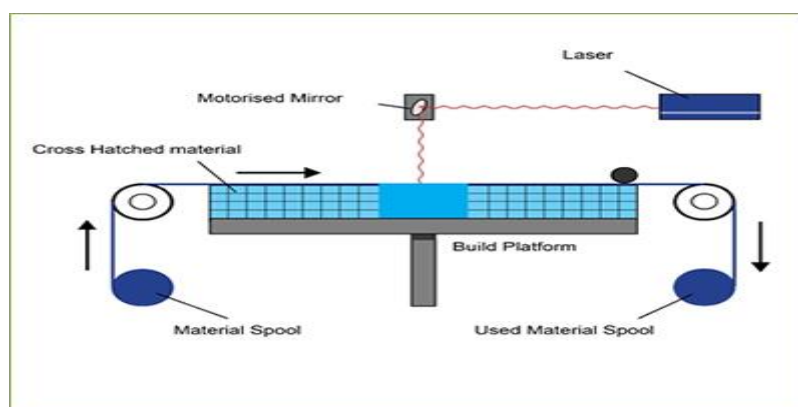


Figure 17 Systematic diagram of Sheet Lamination (*Sheet Lamination | Additive Manufacturing Research Group | Loughborough University, no date*)

5.7 Vat Polymerization (VP)

Vat polymerization is an additive manufacturing method that utilizes liquid photopolymer. It operates by selectively curing liquid polymer in a vat using ultraviolet (UV) light. In this printing method, the building platform extends from the bottom to the top of the resin vat and then descends according to the layer thickness, similar to the PBF process. The photopolymer resin cures layer by layer under UV light and the subsequent layer is built on top of the previous layer. A few printing methods use a moving blade to smooth the layer surface prior to correct construction. The item is ejected from the printer when the vat solution is drained from the building platform. This method is self-supporting, since the liquid vats act as a support for the printing. Additionally, this technique results in a better resolution and smoother surface due to the utilization of liquid building materials. The printing process is influenced by the viscosity of the polymeric resin, which increases as the layer deposition time increases. The systematic flowchart in Figure 18 depicts the vat polymerization process.(Deckers, Vleugels and Kruth, 2014)

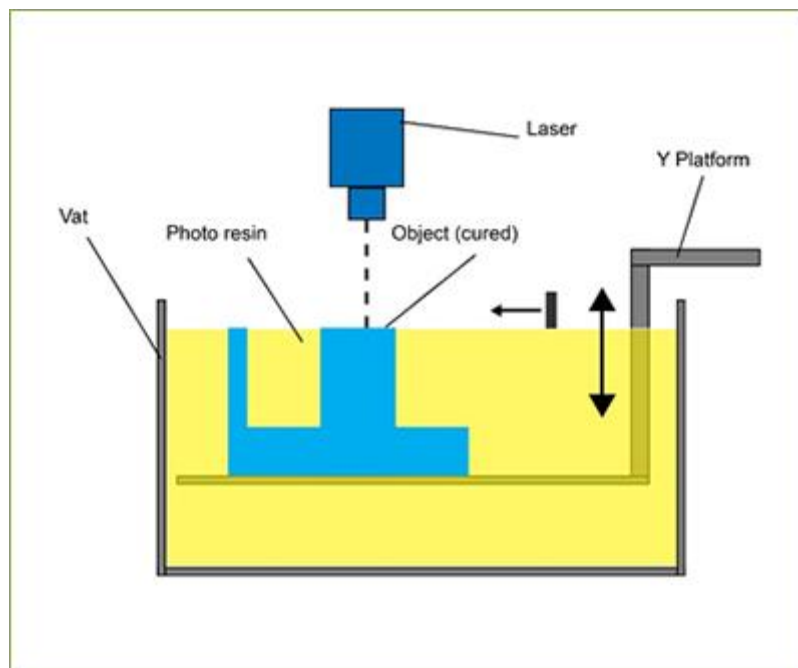


Figure 18 Systematic diagram for vat polymerization (*Sheet Lamination / Additive Manufacturing Research Group / Loughborough University, no date*)

6. Adsorption

Adsorption is a physiochemical mass transfer technique that is commonly used to separate substances from solution or gas phase onto a solid surface via accumulation or concentration rise. Adsorption occurs when atoms or molecules adsorb on a solid surface due to the surface's leftover energy caused by the molecules' uneven attraction.

Indium is often recovered through extraction or leaching from byproducts of zinc manufacturing plants. However, this technology has several disadvantages, including high costs, the generation of large amounts of effluent, chemical waste, and lack of environmental stewardship. Where adsorption is regarded as a long-term solution due to its simplicity and selectivity, as well as its economic and technological practicality.

6.1 Adsorption theory

Adsorption is divided into two types: physisorption and chemisorption, based on the adsorbate and adsorbent's attraction properties. Chemisorption is often a non-reversible process in which adsorbate is held to the adsorbent surface by a chemical bond. Adsorption capacity is dependent on the reactivity of the adsorbent and adsorbate. On the other hand, physisorption occurs through van der Waals contact, which results in the formation of a weak bond. This is a reversible process in which no substantial change in enthalpy is seen. The adsorption capacity of an adsorbent is dependent on the surface charge on the adsorbent and the ionic nature of the adsorbate. The adsorption capacity of a metal is defined as the mass of metals adsorbing per unit mass of adsorbent.

The adsorption capacity (mg/g) is calculated using the following equation. Eq.(5), where metal adsorption from solution by adsorbent is expressed as a percentage of metal removal (%) as indicated in Eq. (6)

$$q_e = \frac{(C_o - C_f) * v}{m} \quad (5)$$

$$\text{REMOVAL \%} = \frac{(C_o - C_f) * 100}{C_o} \quad (6)$$

Here,

q denotes the adsorption capacity in mg/g.

C_o denotes initial concentration in mg/L

C_e denotes equilibrium concentration in mg/L

v represents solution volume in mL

m denotes adsorbent mass in mg

6.2 Adsorption Isotherm

Adsorption isotherms are effective tools for analyzing the adsorption properties of various adsorptive materials. Adsorption is a process that is often used to remove or recover valuable materials from solution and continues until an equilibrium condition is reached. The equilibrium state of adsorption is defined as the amount of adsorbate removed or recovered from solution by per unit mass of adsorbent. Equation (5) mathematically describes the equilibrium state that is used to determine the adsorbent capacity of various adsorbent materials and able to reveal the equilibrium state of the adsorption process. There are many well-established models that have been developed by various scientists throughout time to explain the adsorption behavior of adsorbent. Giles et al. suggested four fundamental isotherm models depending on the shape of the curve: the C isotherm, the L isotherm, the H isotherm, and the S isotherm. (Giles, Smith and Huitson, 1974) Additionally, several concave isotherm models have been developed since a single equation is incapable of adequately explain all mechanisms. Langmuir, Freundlich, Redlich-Peterson, Sips, and Brunauer-Emmett-Teller (BET) are the most often used isotherm models, with an extended version developed for multicomponent systems using the Langmuir equation.

6.2.1 Basic isotherm category

This section will explain the four fundamental kinds of adsorption isotherms as shown in Figure 19. In isotherm plotting, the adsorbent capacity is shown on the Y axis and the equilibrium concentration is plotted on the x axis.

The isotherm of type C: This isotherm model is straightforward, consisting of a linear curve that begins at zero, as shown in Figure 19 (a). This model shows that for every concentration, the ratio of equilibrium concentration to the quantity of compound adsorbing on the adsorbent surface is identical. This is referred to as the distribution coefficient (K_d). This model is suitable for solutions with modest concentration ranges or solutions containing trace pollutants since it provides an approximate notion of adsorption rather than accurately characterizing the reality. The model must be validated before to final usage; else, the real outcome will be distorted. For instance, the limited amount of adsorption sites in a solid adsorbent result in a nonlinear isotherm owing to an endurable saturation plateau.(Giles, Smith and Huitson, 1974)

The isotherm of type L: This adsorption isotherm model appears when the distribution coefficient value (K_d) drops as the solute concentration increases, resulting in the concave curve shown in the Figure 19(b), which indicates the progressive saturation of adsorbent surface. This kind of modeling produces two distinct subgroups: one with a strict plateau, indicating that the adsorbate has a limited amount adsorption site, and another without a strict plateau, indicating that there is no obvious evidence of a limited amount of adsorption sites. However, it is impossible to anticipate whether the adsorbent capacity is limited by this isotherm.

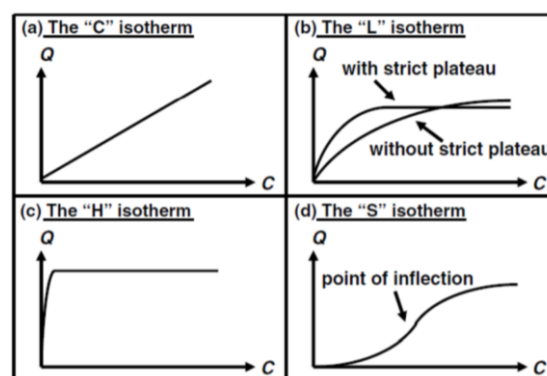


Figure 19 Basic four isotherm type (Giles, Smith and Huitson, 1974)

The isotherm of type H: This isotherm belongs to the L type, in which the initial adsorption slope is unexpectedly greater towards infinity than expected due to the adsorbate's increased affinity for the adsorbents for a specific length of time shown in Figure 19 (c). The cause of this event is likewise inexplicable from a thermodynamic approach.(Tóth, 1994)

The isotherm of type S: This isotherm generates a sigmoidal curve, which serves as an inflection point for at least two counter mechanisms shown in Figure 19 (d) Clay, for example, is an

adsorbent medium, and an adsorbent compound is a combination of nonpolar and other organic compounds, but nonpolar organic compounds having a lower affinity for the clay and adsorbing slowly. Other organic compounds, on the other hand, readily adsorb by the clay once non-polar organic molecules have been absorbed. (Soheila Karimi-Lotfabad, Michael A. Pickard and Murray R. Gray*, 1996) This is known as cooperative adsorption, (Hinz, 2001) and it occurs often in surfactant adsorption. (Smith and Galan, 2002) Due to remnants of metal ligand complex, the presence of metal species in the solution produces this kind of isotherm. During this kind of adsorption, the metal-ligand adsorbs first, followed by the remainder of the complex. (Bolt and van Olphen, 1985)

6.2.2 Langmuir isotherm

The Langmuir isotherm is a well-known model for explaining the equilibrium system of adsorbate and adsorbent when the adsorption process is restricted to one component system. Langmuir developed this adsorption model in 1918 to describe the behaviors of chemisorption processes in which chemical bonds are generated to carry out the adsorption process, particularly ionic bonds. To understand the concept, suppose that the solid has a finite adsorption capacity q_m , that all adsorbent sites are similar, that each adsorbent site can store a single adsorbate, and that each adsorbent site retains energy to maintain adsorbate amount independently. According to the assumption, the adsorption process proceeds as follows. (Langmuir, 2002)

Free adsorbent site + adsorbate compound \rightarrow complex formation on adsorbent surface

According to this assumption, fractional surface coverage is exactly proportional to the rate of desorption, and in the equilibrium state the adsorption and desorption are equal shown in Eq.(7)

$$k_a C_e (1 - \theta) = k_d \theta \quad (7)$$

Where k_a stands for the adsorption rate constant, k_d for the desorption rate constant, and C_e (mg/L) for the equilibrium concentration.

The following equation represents more formal form of Langmuir equation (8):

$$\theta = \frac{q}{q_m} = \frac{K_L C_e}{(1 + K_L C_e)} \quad (8)$$

Where,

$$K_L = \frac{k_a}{k_d} \quad (9)$$

The adsorbent capacity is denoted by q , while the quantity of adsorbate held on the adsorbent surface in a single monolayer is denoted by q_m (mg/g) (alternatively called maximum adsorption capacity).

In general, the Langmuir isotherm model assumes that each adsorbate chemical occupies its own adsorbent site and that there is no interaction between two neighboring compounds on a homogenous surface. The following are the nonlinear Eq.(10)(11) and linear equations for the Langmuir isotherm model:

$$q_e = \frac{q_m K_L C_e}{(1 + K_L C_e)} \quad (\text{non - linear form}) \quad (10)$$

$$\frac{1}{q_e} = \frac{1}{K_L q_m C_e} + \frac{1}{q_m} \quad (\text{Linear form}) \quad (11)$$

Where, q_e (mg/g) is the concentration of adsorbate in the surface of adsorbent in the equilibrium state and K_L (L/mg) denotes the Langmuir constant.(Liu *et al.*, 2019)

Another significant factor in the Langmuir isotherm is the factor of separation or equilibrium parameter, which is denoted by R_L and can be expressed as

$$R_L = \frac{1}{1 + K_L C_o} \quad (12)$$

Where C_o signifies the initial concentration of the solution, and the R_L value is used to assess the Langmuir model's fit for the adsorption process. R_L value more than one indicates an unfavorable process, whereas a value greater than zero or less than one indicates a favorable process, and R_L value of zero indicates an irreversible process (Wang, Wang and Ma, 2010).

6.2.3 Freundlich isotherm

The concave isotherm model in the form of L or H is frequently used. Freundlich developed an empirical model for isotherm modeling in 1909, based on the following relationship between adsorbate concentration on adsorbent and solute concentration shown Eq. (13) & (14):

$$q_e = K_F C_e^{1/n} \text{ (Nonlinear form)} \quad (13)$$

$$\log q_e = \log K_F + \frac{1}{n} \log C_e \text{ (Linear form)} \quad (14)$$

Where q_e (mg/g) is the adsorbate concentration in the adsorbent phase, C_e (mg/L) is the adsorbate equilibrium concentration in aqueous solution, K_F is a constant that indicates the adsorbent's relative adsorption capacity, and $1/n$ is the adsorption intensity, where a higher fractional value indicates a more energetic site on the adsorbent, and n values between 1 and 10 are favorable for adsorption.

This model overcomes the Langmuir isotherm model's limitations in that it is applicable to both homogeneous and heterogeneous adsorption surfaces and can be used for both chemisorption and physisorption. Additionally, the Freundlich isotherm offers a simple mathematical formula rather than interpreting the theoretical assumption of heterogeneous energy for active adsorption sites. This equation is applicable to the majority of the adsorption field and has shown more practicality than the other isotherm models. (Xu, Cai and Pan, 2013) However, the impact of temperature on the adsorption process is difficult to describe in this model because as solution concentration increases, mass on the adsorbent surface decreases. The Freundlich isotherm cannot be used to estimate adsorption at high solute concentrations since it was developed for low solute concentrations. Adsorption increases as q_e increases, but n is always higher than 1, thus the rise is not significant. This model is often used to describe systems with multiple components and heterogeneous adsorption. Calculated slope range can be used to determine the heterogeneity of the adsorbent surface; a value closer to zero indicates more heterogeneity. (Foo and Hameed, 2010)

6.2.4 Sips isotherm

Sips isotherm is a hybrid of Langmuir and Freundlich isotherms that changes its behavior in response to changes in the adsorbate concentration. This model behaves like a Freundlich

isotherm at low adsorbate concentrations and like a Langmuir isotherm at high adsorbate concentrations, assuming monolayer adsorption.(Foo and Hameed, 2010) Changes in process parameters like as pH, temperature, and adsorbate concentration change the isotherm model.(Sips, 2004) The Sips isotherm is represented by the following equations. Eq. (15) nonlinear & (16) linear form.

$$q_e = \frac{K_s C_e^{\beta_s}}{1 + a_s C_e^{\beta_s}} \quad \text{(Nonlinear form)} \quad (15)$$

$$\beta_s \ln(C_e) = -\ln\left(\frac{K_s}{q_e}\right) + \ln(a_s) \quad \text{(Linear form)} \quad (16)$$

Where K_s is the Sips affinity constant (L/mg) and a_s is the isotherm's exponent, which denotes the surface heterogeneity and affects the model's behavior; values close to 1 indicate that the model behaves like a Langmuir isotherm, while values greater than 1 indicate that the model behaves like a Freundlich isotherm.

6.3 Adsorption Kinetics

Adsorption is a physiochemical process, and adsorption kinetics predict the mass transfer rate of the adsorbate to the adsorbent, which provides a complete adsorption mechanism for batch adsorption.(B *et al.*, 2011) Adsorption kinetics consists of two consecutive phases: the first phase involves the fast transfer of adsorbate molecules to the adsorbent surface, followed by the second phase, which involves the gradual attainment of equilibrium. Adsorption kinetics quantifies the rate at which solute particles adsorb on the adsorbent, which is directly related to the adsorption efficiency. The rate constant values are determined using the batch kinetic models for adsorption.

According to the (Plazinski, Rudzinski and Plazinska, 2009) assumption adsorbate molecule follows four sequential steps for adsorption process.

- the adsorbate is carried inside the bulk in solution
- the adsorbate is transported crosswise and liquid film clasping the adsorbent
- the adsorbate is transported though the pore of adsorbent by diffusion.
- the adsorbate is attracted by the adsorbent surface and adsorption occurs

6.3.1 Pseudo first-order model

Several models were created to better explain the adsorption mechanism in batch adsorption. Lagergren derived the pseudo-first order empirical equation in 1898 on the basis of the assumption that the change in adsorbate uptake rate with time is exactly proportional to the differential equilibrium concentration and the adsorbate accumulates on the adsorbent surface. (Ho and McKay, 1999) Typically, a kinetic model is utilized to deduce the adsorption kinetic data from a batch adsorption process. The following is a simple derivation of pseudo first-order and Eq.(21) is considered as final form:

$$\frac{dq}{dt} = k_1(q_e - q) \quad (17)$$

$$(q_e - q) dq = k_1 dt \quad (18)$$

Integrate the eq.(18)

$$\int_0^{q_t} \frac{1}{(q_e - q)} dq = \int_0^t k_1 dt \quad (19)$$

$$\ln(q_e - q_t) = \ln(q_e) - k_1 t \quad (20)$$

$$\log(q_e - q_t) = \log(q_e) - \frac{k_1}{2.303} t \quad (21)$$

Where q_e (mg/g) represents the equilibrium adsorption capacity and q_t (mg/g) signifies the adsorbent adsorption from solution at time t (min), and K_1 is the constant determined by the equation.

6.3.2 Pseudo second-order model

Ho and McKay's equation was used to create a pseudo second order model equation.(Ho and McKay, 1999) Chemisorption, which includes the exchange of electrons between adsorbate and adsorbent under the influence of valance force, is the rate-determining or rate limiting step in this kinetic model.(Robati, 2013) The following Eq. (22) is the derivation:

$$\frac{dq}{dt} = k_2(q_e - q_t)^2 \quad (22)$$

Where, K_2 is the coefficient of pseudo second order rate, by taking integration in Eq. (22) by using following limit when $t=0, q_t=0$ and $t=t, q_t = q_t$

$$\int_0^{q_t} (q_e - q_t)^{-2} dt = \int_0^t k_2 dt \quad (23)$$

$$-\frac{1}{(q_e - q_t)} + \frac{1}{q_e} = k_2 t \quad (24)$$

$$q_t = k_2 t q_e^2 - k_2 t q_t q_e \quad (25)$$

The following equation(26) is a liner form of this model

$$\frac{t}{q_t} = \frac{1}{k_2 q_e^2} + \frac{1}{q_e} t \quad (26)$$

The K_2 values is obtained from plotting $\frac{t}{q_t}$ vs. t that called as rate constant.

6.3.3 Intraparticle diffusion model

The interparticle diffusion model was used to evaluate the relationship between the mechanism of diffusion and the kinetic influence on the adsorption process. The build diffusion model considers that the adsorbent framework is porous so that adsorbate can diffuse through the pore. Several publications have previously revealed that the adsorption rate is influenced by intraparticle diffusion. Weber and Morris developed a liner equation model (27) to calculate the initial rate of interparticle diffusion. (Tanhaei *et al.*, 2015)

$$q_t = k_i t^{1/2} + C \quad (27)$$

Where C represents the intercept that denotes the thickness of boundary and K_i the interparticle diffusion rate constant ($\text{mg/g min}^{1/2}$).

The interparticle model is derived by graphing the adsorbate concentration, q_t vs $t^{1/2}$, with intercept value 0 indicating the rate limiting steps. When the plot does not pass through the origin, the intraparticle model behaves similarly to other kinetics models and acts as a rate controlling factor.(Yakout and Elsherif, 2010)

It is evident that the interparticle adsorption rate increases with rising temperature as pore diffusion increases, and as a result, the K_i value increases with increasing solution temperature.(Yakout and Elsherif, 2010)

6.4 Error Analysis

Several linear isotherm equations are often employed to deduce the behavior of the adsorption process. The correlation coefficient of the regression is used to assess the experimental data for linear isotherm model fitting, with R^2 values close to 1 indicating a more accurate fit to the model.

The data transformation, normalization, is often used to linearize the adsorption isotherm by modifying the error structure; furthermore, the conventional least squares approach violates the premise of normality and variation of error.(Myers, 1990) However, in certain instances, nonlinear transformations, (Malek A., Farooq, 1996) such as Gauss-Newton or Leven-berg-Marquardt, are used instead of linear transformations on the isotherm data. (Hanna, O. T., Sandall, 1995) To optimize equilibrium experimental data, an error function must be defined to assess the isotherm fitting for adsorption. Five distinct error functions will be used in this thesis effort to minimize the error range of isotherm data using the solver add-in for Excel. The following error function is described in detail.

6.4.1 The sum of the square of the error (ERRSQ)

This error function is often used to optimize isotherm data for adsorption.(Mane, Deo Mall and Chandra Srivastava, 2007) The ERRSQ function is represented by the following equation (28):(Ng, Cheung and McKay, 2002)

$$ERRSQ = \sum_{i=1}^n (q_{e \text{ exp}} - q_{e \text{ model}})^2 \quad (28)$$

Where $q_{e \text{ exp}}$ indicates the concentration of adsorbate on the adsorbent surface determined experimentally, and $q_{e \text{ model}}$ denotes the concentration of adsorbate on the adsorbent surface determined theoretically using an isotherm model.

The main drawback of this error function is that, while it provides better fitting of the model by magnitude, the error and error rise by square at the same time, resulting in larger end of concentration range.(Ng, Cheung and McKay, 2002)

6.4.2 The hybrid functional error function (HYBRID)

Kapoor and Yang established the hybrid fractional error function (HYBRID) to compensate for the absence of an ERRSQ function capable of operating at low concentrations. The function is generated by dividing the experimental adsorbate concentration on the adsorbent surface with 100 divided by the number of data points (n) minus the parameter number. (Kapoor and Yang, 1989) HYBRID error function is represented by the following expression Eq. (29).

$$HYBRID = \frac{100}{n-p} \sum_{i=1}^n \left[\frac{(q_{e \text{ exp}} - q_{e \text{ model}})}{q_{e \text{ exp}}} \right] \quad (29)$$

6.4.3 The sum of absolute errors (EABS)

This equation is similar to ERRSQ but has been changed to provide a better fit than ERRSQ by raising the amount of error, which favors data with a high concentration.(Kundu and Gupta, 2006) EABS error function is represented by the following expression Eq. (30).

$$EABS = \sum_{i=1}^n |q_{e \text{ exp}} - q_{e \text{ model}}| \quad (30)$$

6.4.4 The average relative error (ARE)

Marquardt pioneered the development of the average relative error function. This function is capable of minimization of the fractional error distribution throughout the whole concentration range. ARE function is denoted by the following expression Eq.(31).(Marquardt, 2006)

$$ARE = \frac{100}{n} \sum_{i=1}^n \left(\frac{|q_{e \text{ exp}} - q_{e \text{ model}}|}{q_{e \text{ exp}}} \right) \quad (31)$$

6.4.5 Marquardt's percentage standard deviation (MPSD)

This error function is analogous to the geometric mean error distribution, but it has been modified using the degree of freedom of the system to improve its accuracy. (Ng, Cheung and McKay, 2003) MPSD error function is represented by the following equation (32).

$$MPSD = \frac{1}{n-p} \sum_{i=1}^n \sqrt{\left(\frac{(q_{e \text{ exp}} - q_{e \text{ model}})}{q_{e \text{ exp}}}\right)^2} \quad (32)$$

7. Experimental Procedure

The adsorption experiments for Indium were done in batch mode. To begin, batch experiments were done utilizing granular ion exchange resin to evaluate the materials' Indium adsorption behavior. The following parameters are investigated to better understand the adsorbent's adsorption mechanism: effect of pH, the influence of contact time, the effect of starting concentration, and the equilibrium isotherm (Sekhararaogulipalli, Prasad and Wasewar, 2011). The entire method (shown in Figure 22) was followed in this thesis for adsorbent materials (Lewatit TP-207, Lewatit TP-260, and Amberlite IRA 742) in order to evaluate the functionality of Indium adsorption and the optimal adsorption parameters. Later on, the Indium adsorption functional materials were selected by a batch adsorption procedure, and the materials were used to fabricate a 3D printed adsorbent module for use in the study. The batch adsorption and recovery method for Indium was carried out, as well regeneration study of a 3D printed adsorbent module.

The weight of all solid materials used in dosing was determined using a standard scale (METTLER AE240), whereas liquid samples and reagents were determined using an electronic pipette (Sartorius). The pH of the adsorbate-containing solution was adjusted, and the solution temperature was measured using a Metrohm 744 pH meter. All adsorption experiments were conducted in batch mode at room temperature. The solution was mixed with a constant rotation speed using an EDMUND BULER KS10 shaker (300 rpm).

Following each batch adsorption of granular ion exchange resin, the adsorbent was removed from the solution using a syringe filter with a pore size of $0.20\mu\text{m}$ and a diameter of 26mm. The filtrated samples were promptly refrigerated until ICP measurement. The metal ion concentration in solution was determined by ICP analysis with an AGILENT TECHNOLOGIES 7900. This thesis work investigated the adsorbent's selectivity for the Indium ion. All experiments and analyses were conducted at the chemical laboratory at LUT.

7.1 Materials and Methods

This chapter will describe the materials used in the whole thesis work and methods used for carrying out the research work.

7.1.1 Reagents and chemicals

The following materials were used in this thesis work Lewatit® TP-207, Lewatit® TP-260, Amberlite® IRA-743 and Nylon 12 were used that purchased from Sigma Aldrich. Indium AAS standard nitric acid base 1000ppm stock solution was utilized to prepare synthetic solution for batch adsorption. NaOH and HNO₃ of analytical grade were employed to alter the pH of the solution, while concentrated HCl was used to regenerate and recover Indium from the adsorbent surface. All reagents were of analytical grade and required no additional purification.

7.1.2 Additive manufacturing process

The process of additive manufacturing was utilized for producing 3D printed adsorption modules that begun with the design of the 3D object to be printed. AutoCAD software was used to design the desired 3D object. The obtained three-dimensional pictures were processed with the Cura software to transform them into workable forms (G-code) for the printer, which is a kind of instructions for the printer's printing process. The 3D object was manufactured with the ShareBot SnowWhite2 SLS 3D printer. The printing process requires the adjustment of printing parameters in order to obtain a quality 3D printed product. Several batch runs were conducted in order to determine the optimal printing parameters for nylon 12 and ion exchange resin. The optimal parameters were as follows: powder control mode with a building plate temperature of 156, 33% laser power, a scanning rate of 2200 mm/s, and a layer thickness of 0.2 mm. The resulting three-dimensional object was cleaned by carefully removing unsintered powder from the structure prior to initiating the adsorption procedure. The produced adsorbents did not require additional treatment. The Figure 20 shown the 3D printed adsorbents and granular adsorbent.

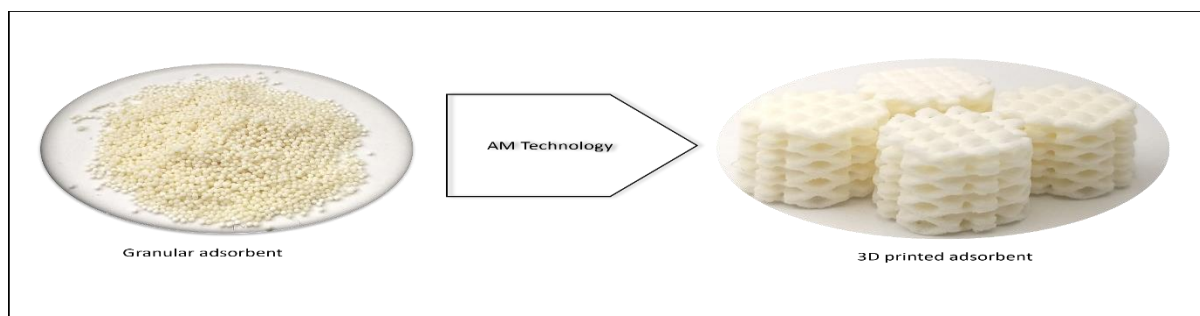


Figure 20 Typical and 3D printed adsorbent

7.1.3 Preparation of Indium solution

The solution with the required Indium concentration was produced using a 1000ppm AAS Indium standard solution. The solution was diluted with water to meet the requirements of the kinetic and isotherm batch adsorption experiments.

7.1.4 pH dependency experiment

pH has a significant effect on the adsorption and desorption processes of ion exchange resin due to the protonation and deprotonation effects that occur at various pH levels. To investigate the influence of pH on the adsorption process, the pH value was changed while the Indium solution concentration (100ppm), adsorbent dose (0.001g/ml), and temperature remained constant (room temperature) and maintained 500rpm shaking speed for 24h for achieving equilibrium stage of adsorbent. The experimental pH value ranges were 1-4, as explained by the Eh-pH diagram described by Assefi et al. Figure 21 illustrates the Eh-pH diagram. The diagram depicts the transition of Indium as a function of pH, with three distinct forms of Indium seen at various pH values: InCl_3 , $\text{In}(\text{OH})_3$, and In (s). According to the figure, the Indium adsorption range is 1-4, since Indium is present in the chloride form in this region. However, at lower pH values (0.5-1.5), the hydronium ion form inhibits adsorption due to the reduced amount of adsorption sites. Above pH 4, Indium forms $\text{In}(\text{OH})_3$, which settles as a precipitate that the adsorbate may not absorb. (Assefi *et al.*, 2018a)

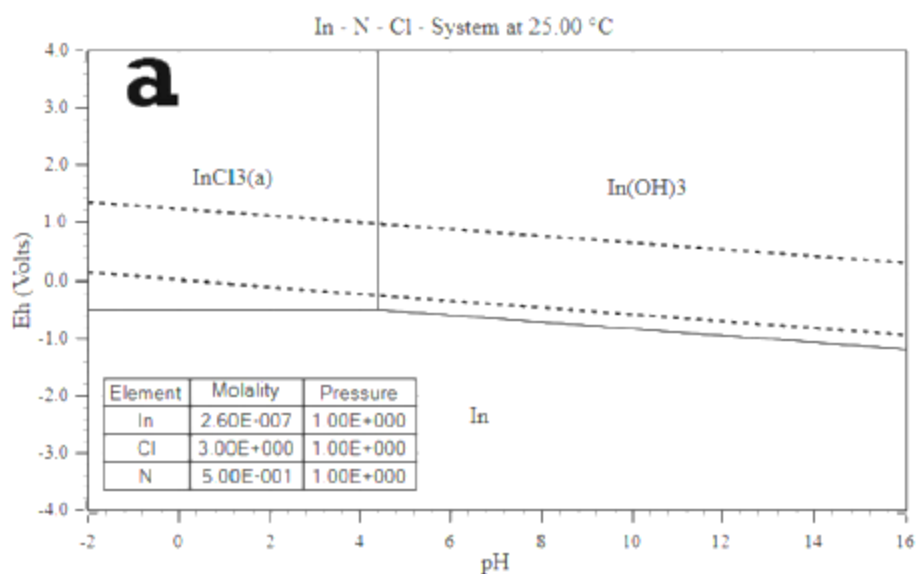


Figure 21 The Eh-pH diagram for Indium (Source: (Assefi *et al.*, 2018a))

7.1.5 Batch adsorption procedure

An illustration of batch adsorption process is shown in Figure 22. The optimal pH values were determined using the pH dependence test with 100ppm Indium solution primarily to examine the adsorption isotherms and kinetics, which indicated that the optimal pH value was 3.5. The various concentrations of Indium solution ranging from 5-200 ppm were produced in accordance with the optimal pH for adsorption batch tests in order to observe the initial concentration effect on the adsorption and determine adsorbent's maximum adsorption capacity (Sekhararaogulipalli, Prasad and Wasewar, 2011). A 10 mL solution of Indium was taken in a 10 mL disposable plastic tube with a granular adsorbent dose of 0.001/mL. The adsorption period was 24 hours when the shaker was set at a constant speed of 500 rpm (Assefi *et al.*, 2018b). Following adsorption, the adsorbent was removed from the solution using a syringe filter and the solution was preserved for ICP analysis. The same batch adsorption process followed for 3D printed adsorbent modules except the filtration removal process of adsorbent from solution. The capacity of Indium for adsorption was determined using eq. (5) (Assefi *et al.*, 2018b)

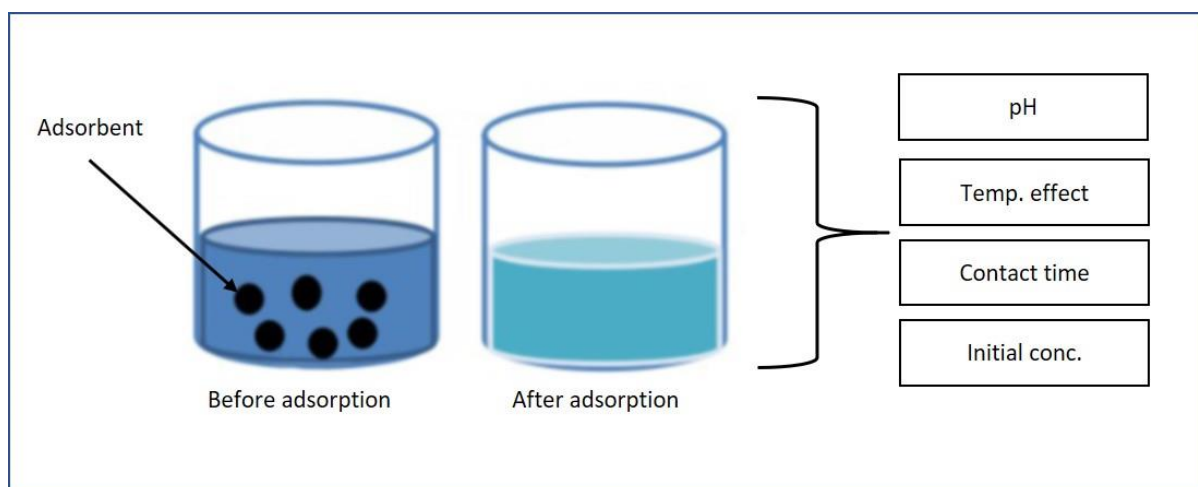


Figure 22 Adsorption in batch mode

The kinetic study used a constant concentration of 50ppm (granular adsorbent), 150ppm (3D printed adsorbent module) a pH of 3.5, and a constant temperature while changing the adsorption duration (5min-1440min for granular adsorbent and 2.5min-360min for 3D adsorbent module). The batch adsorption technique is identical to the isotherm adsorption procedure for granular adsorbents.

7.1.6 Indium recovery from brine and regeneration

The Indium was recovered using a fixed bed column adsorption preconcentration technique from a seawater brine solution (composition stated in the Table 1).

Table 1 Seawater brine composition

Element	Concentration (mg/L)
Na ₂ SO ₄	1.521
NaCl	193.863
KCl	5.178
MgCl ₂	4.569
CaCl ₂	0.275
B	37.021
Li	1.60
In	0.076
Rb	1.688
V	0.2746
Ga	0.1062
Sc	0.0682
Mo	0.0934

Figure 22 illustrates the systematic diagram of the basic column operation for preconcentration. Four pieces of 3D printed adsorbent modules were dosed into a glass column with a diameter of 15mm and a height of 100mm, and cotton was inserted into the glass column's inlet and outlet to provide filtering support. The brine was fed into the top of the column at a constant flow rate of 3ml/min (batch total volume 500ml) using a peristaltic pump (Masterflex L/S). Due to the gravitational and pumping forces, the liquid passes through the adsorbent module and adsorption occurs. A small quantity (10-15ml) of pH 0.5 acid containing HCL was passed down the column, which extracts Indium from the adsorbent and collects it as effluent from the adsorbent column. The collected solution contained concentrated solution of In(III) and the quantity was confirmed by ICP analysis. The recovery and regeneration processes occurred concurrently with the assistance of HCL acid elution. (Repo, Warchoł and Sillanpää, 2017)

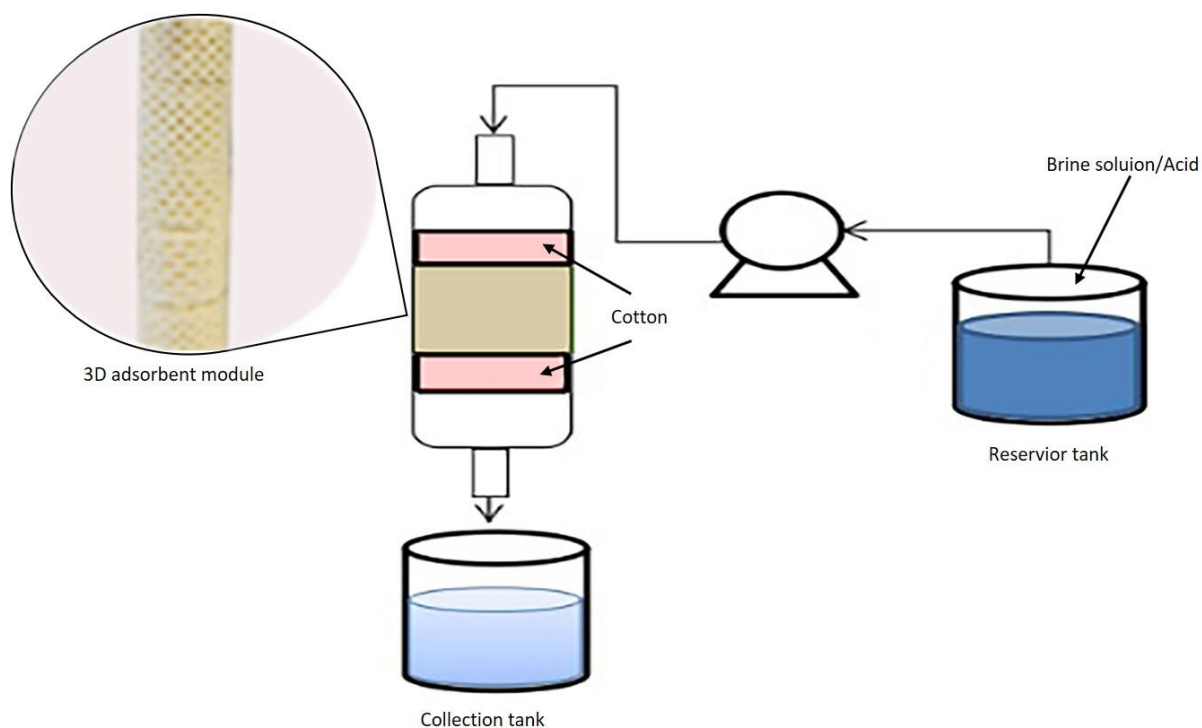


Figure 23 Indium recovery from brine and regeneration process

7.2 Adsorbent Characterization

The following instruments were utilized for characterizing the adsorbent: Fourier Transform Infrared Spectroscopy and Scanning electron microscopy.

7.2.1 Fourier Transform Infrared Spectroscopy (FTIR)

The surface functionalities of all adsorbents were determined before and after the adsorption process using a Perkin Elmer Frontier Spectrometer equipped with an ATR module in order to determine the changes caused by metal adsorption on the adsorbent surface. All samples were measured with a resolution of 1 cm^{-1} in the $4000\text{-}400 \text{ cm}^{-1}$ wave length infrared area. The solution concentration of 200 ppm and the pH of the solution were used as controls while preparing the FTIR samples after adsorption. The 3D printed adsorbent is composed of 10% ion exchange resin and 90% nylon 12 powder for the purpose of detecting changes in nylon 12 powder and ion exchange resin during AM manufacturing. The granular adsorbents were directly introduced to the FTIR equipment, but for measuring the FTIR 3D printed adsorbents, a thin slice of the structure was sliced from the main structure and analyzed.

7.2.2 Scanning Electron Microscopy

The adsorbent's morphology was studied using the available SEM instrument at LUT University, model Hitachi SU 3500, which combines with EDS analysis. Adsorbent samples were prepared prior to and after adsorption in accordance with SEM's standard operating procedures for morphology and elemental analysis. The high vacuum condition was employed for the SEM analysis, and the acceleration voltage was 15KV.

8. Result and Discussion

This chapter will discuss the results of the experiments and analyses conducted in this thesis on the adsorption process and recovery of Indium from seawater brine.

8.1 Effect of pH

The pH of the adsorption process is a critical parameter that must be checked before proceeding with the adsorption experimentation to any further extent. The pH has an effect on the surface charge of the adsorbent due to protonation and deprotonation, and it also has an impact on the adsorbed element at high levels. The TP-207 demonstrated the influence of pH on the Indium adsorption process in the Figure 24. As shown in the picture, the highest adsorption capacity was discovered at pH 3.5 to 4, with pH 3.5 being selected as the best pH for further investigation. Above 3.5 pH, the In (III) ion precipitates out as $\text{In}(\text{OH})_2$, which does not adsorb onto the adsorbent (Assefi *et al.*, 2018b). This is why the ideal pH was determined to be 3.5. The remaining adsorbents (TP-260 and IRA-743) were utilized in the same pH range for the continuation of the experiment since a previous investigation revealed that the highest adsorption capacity was found for those adsorbents at pH 3.5 (Assefi *et al.*, 2018b).

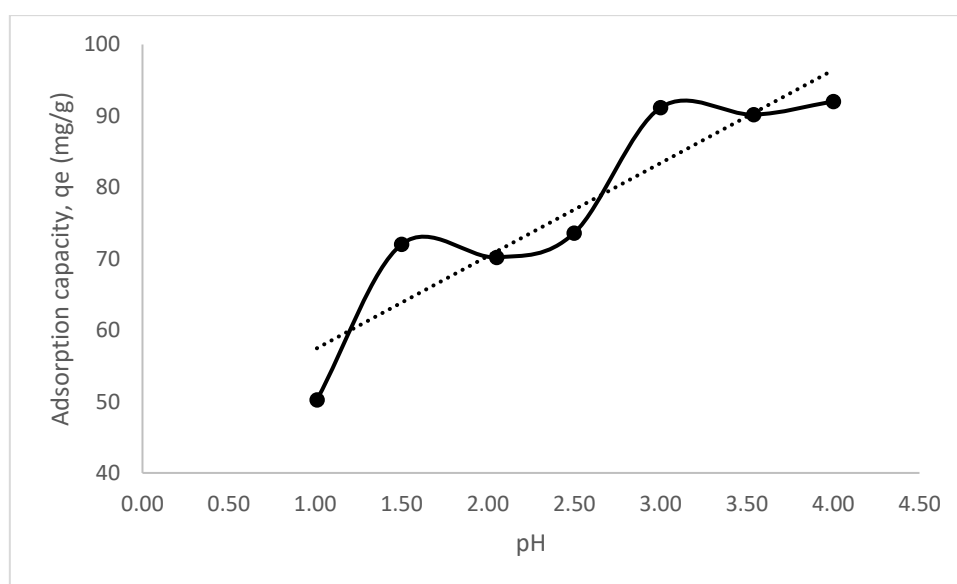


Figure 24 pH effect on In (III) adsorption by resin TP-207 at room temperature, 24h contact time and 500 rpm shaking speed.

Resin TP-207 is a cation exchange resin by nature, which decreases the pH of the solution during the adsorption process by releasing H^+ ions into the solution. The following Figure 25 illustrates the pH reduction of pH values ranging from 1 to 2.5, indicating the increase in proton concentration in the solution. While the pH value increases over the range during adsorption, it indicates an increase in the amount of hydroxyl ion in the solution.

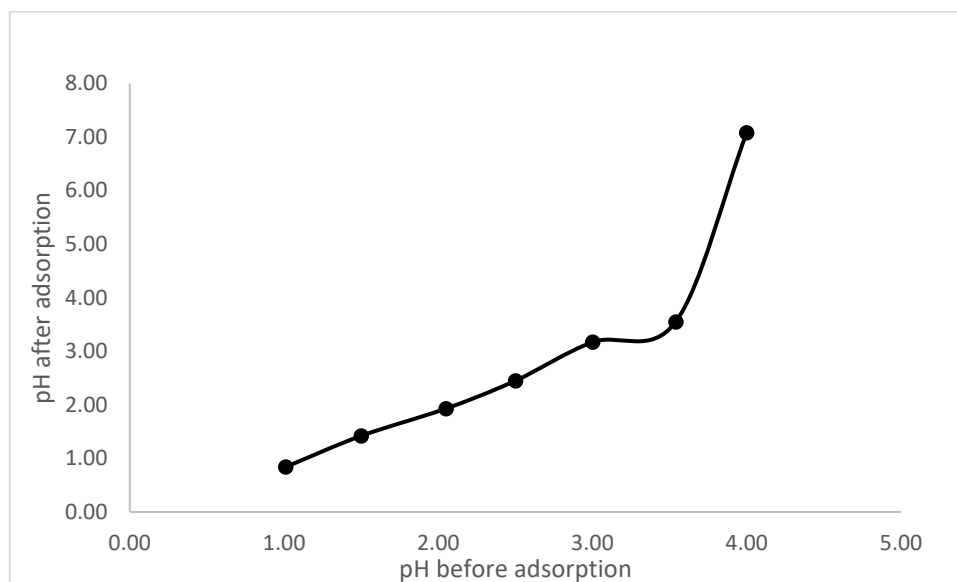


Figure 25 Final vs Initial pH of adsorbed solution

Metal adsorption at a lower pH is advantageous because the concentration of the H^+ ions is higher, which normally creates competition with the metal ion. (Setiawan, Sakamoto and Shiratori, no date) Adsorption increased as the pH value increased, as indicated in the Figure 24. However, the increased pH proved detrimental to In(III) adsorption process due to the generation of $In(OH)_3$. (Assefi *et al.*, 2018b)

8.2 Effect of contact time

Contact time has an effect on the adsorption process and is connected to the adsorption rate or kinetic studies. The purpose of this study was to determine the time necessary for the adsorbent to attain its maximum adsorption capacity and the rate of In(III) recovery on the adsorbent surface. The study used four separate adsorbents (TP-207, TP-260, IRA-743, and 3D printed TP-260) to compute the adsorption capacity q_t over a range of time intervals. For TP-207, TP-260, and IRA-743, the adsorbed concentration was 50 ppm, the temperature was 25 C, the shaking speed was 500 rpm, and the contact time interval was 0-720 min; for 3D printed TP-260, the contact time interval was 0-360 min, the adsorbent concentration was 150 ppm, and

the same temperature and shaking time were used. The Figure 26 depicts the effect of contact time on the various adsorbents employed in the experiment.

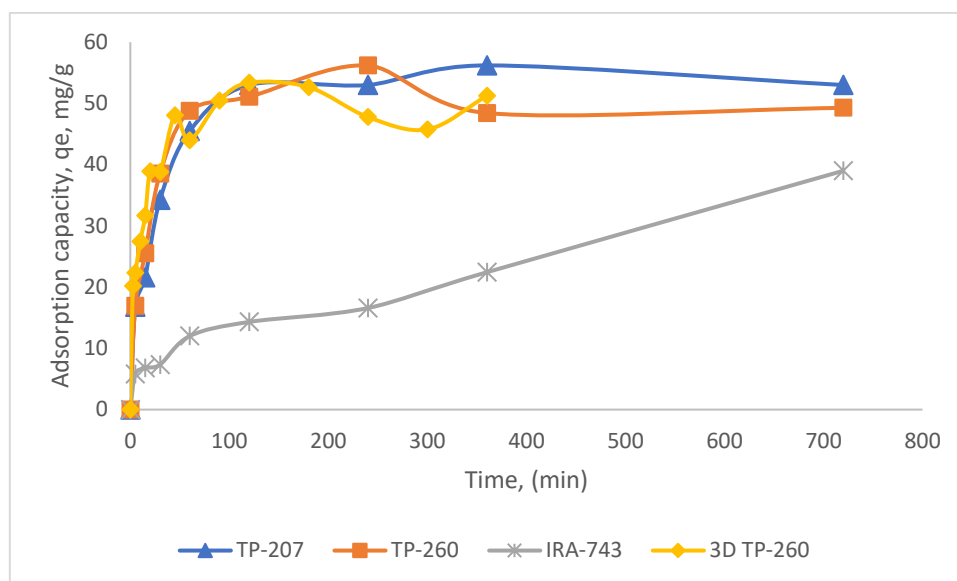


Figure 26 Effect of contact time on Indium adsorption process onto TP-207, TP-260, IRA-743 and 3D printed TP-260; temperature 25°C, shaking speed 500 rpm, initial concentration 150ppm for 3D TP-260 and other 50ppm initial concentration.

As can be observed from the curve, adsorbent TP-207 begins adsorption of In(III) immediately upon contact. The absorption of In(III) from adsorbed solution increased substantially until 120 min, reaching adsorption capacity 53 mg/g, and then remained stable until 720 min. While adsorbent TP260 followed the same time-dependent adsorption profile as its partner until 60 minutes, at which point adsorption capacity increased steadily to 56 mg/g to time 240 minutes. Following that time point, adsorption capacity decreased marginally and remained steady for the remainder of the time span. The 3D printed TP-260 adsorbent followed the same pattern as the TP-260 adsorbent and achieved a maximum adsorption capacity of 53mg/g at 120 minutes, slightly greater than the TP-260 adsorbent. After that period, the adsorption capacity decreased somewhat and then steadily increased after 300 minutes. The time-dependent adsorption profile of IRA-743 demonstrated that Indium was gradually absorbed from the adsorbed solution over time and achieved a maximum adsorption capacity of 39 mg/g at 720 min.

8.3 Kinetic analysis

This section contains kinetic calculations for four different adsorbents that were used in the experiment. Modelling was applied to experimental data using a pseudo first order, pseudo

second order reaction linear kinetic models, and a non-linear interparticle model, but the intraparticle model did not fit with the experimental data.

8.3.1 Pseudo first order and pseudo second order kinetic model

The pseudo-first order and pseudo-second order adsorption kinetic models are extensively employed in the research of sorption (Ho and McKay, 1999). For each adsorbent, the pseudo first order and pseudo-order kinetic models are applied to the experimental data and shown together in a single curve. Pseudo first order reaction kinetic model: using equation (20), plot $\ln(q_e - q_t)$ versus t to obtain the pseudo first order adsorption kinetic model and the adsorption rate related to the number of unoccupied adsorptive sites.

A pseudo-second order adsorption kinetic equation was constructed utilizing the square product of the difference between the available adsorptive site and the occupied site on the adsorbent surface (Ho and McKay, 1999). Equation (26) denotes a pseudo-second order kinetic model that was utilized to plot the model (t/q_t versus t) experimentally. The pseudo first order and pseudo second order adsorption kinetics for each adsorbent are depicted in Figure 27-30

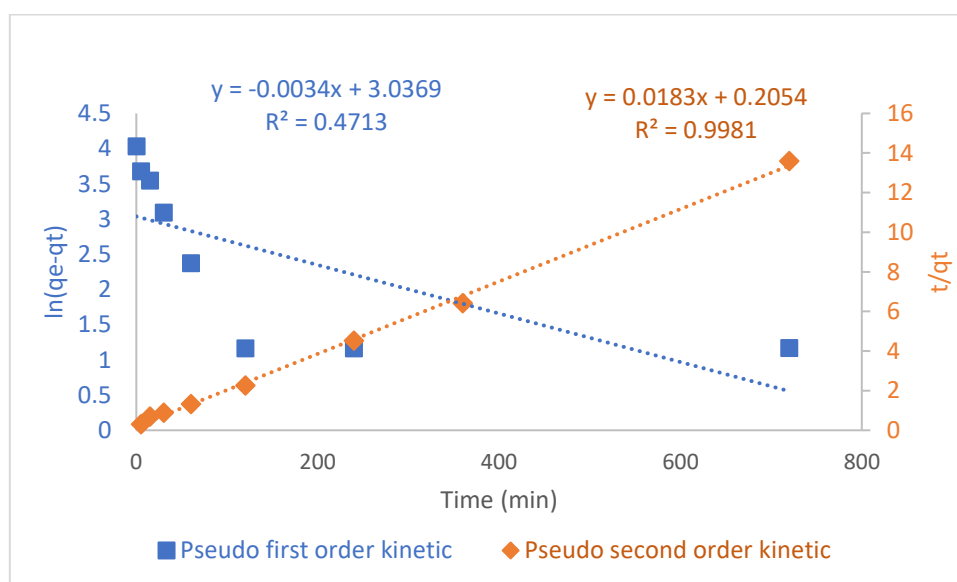


Figure 27 In(III) adsorption pseudo first order and pseudo second order kinetic model for TP-207 adsorbent; 50ppm initial concentration, 500rpm shaking speed.

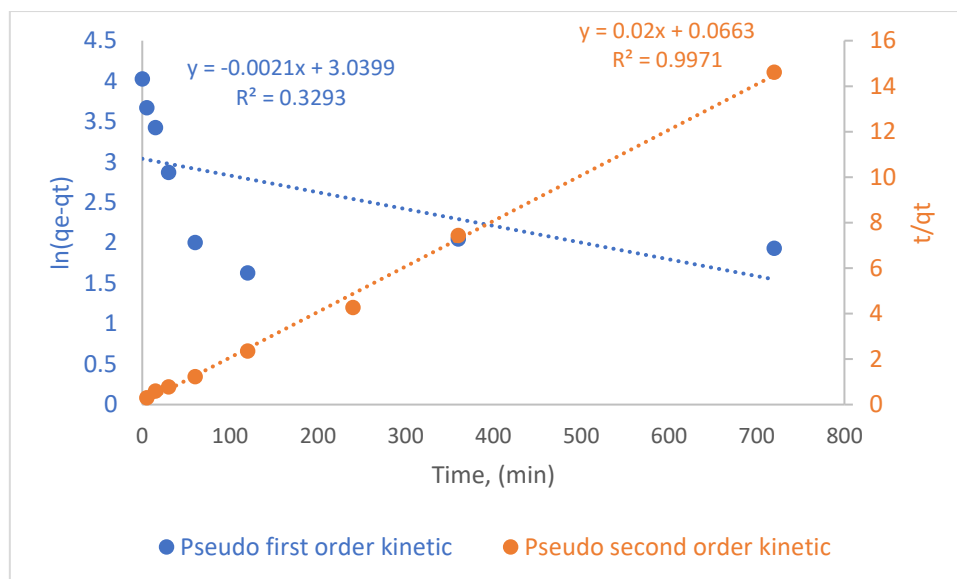


Figure 28 In(III) adsorption pseudo first order and pseudo second order kinetic model for TP-260 adsorbent; 50ppm initial concentration, 500rpm shaking speed.

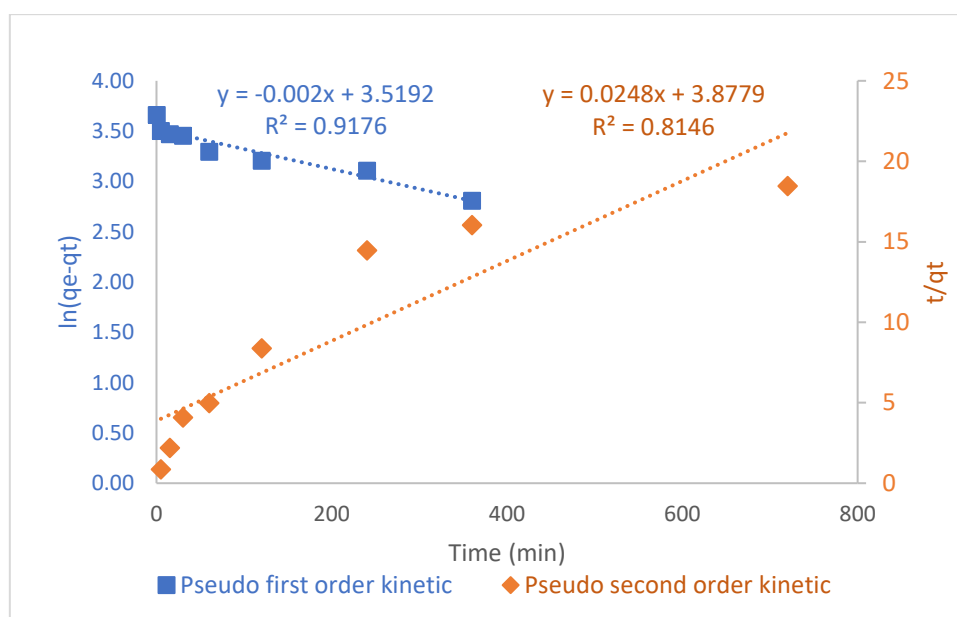


Figure 29 In(III) adsorption pseudo first order and pseudo second order kinetic model for IRA-743 adsorbent; 50ppm initial concentration, 500rpm shaking speed.

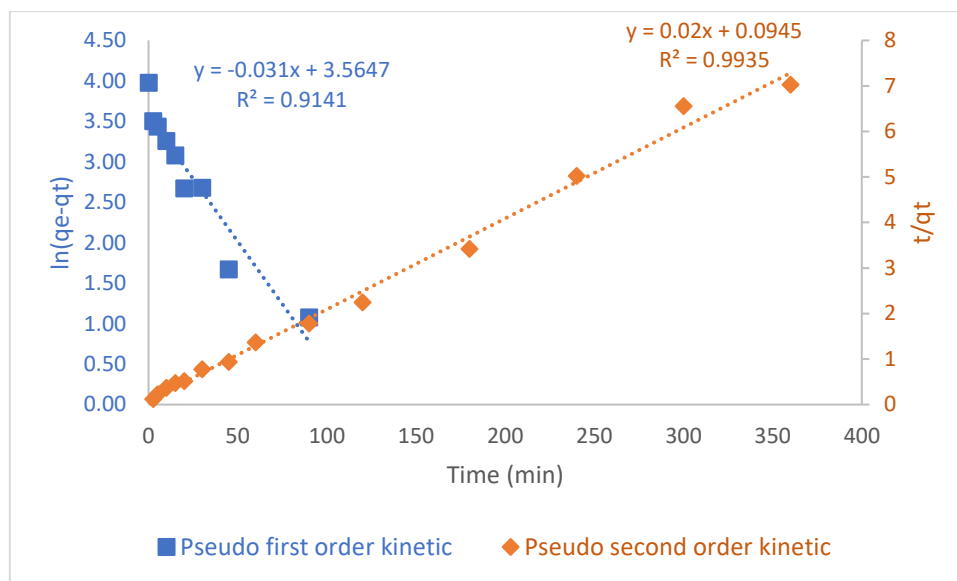


Figure 30 In(III) adsorption pseudo first order and pseudo second order kinetic model for 3D TP-260 adsorbent; 50ppm initial concentration, 500rpm shaking speed.

The models generated the parameter and constant values shown in Table 2. The coefficient of determination (R^2) values is utilized to assess the model's appropriateness. According to the comparison of R^2 values, the pseudo second order adsorption kinetic model is suitable for three adsorbents (TP-207, TP-260, and 3D TP-260), whereas the pseudo first order reaction kinetic model is more suitable for the adsorbent IRA-743. However, because the deviation of the pseudo-second-order model predicted and experimental values was less than that of the pseudo-first-order kinetic model, it may be concluded that IRA-743, like the other three adsorbents, followed second order kinetics.

Table 2 Pseudo first and pseudo second order kinetic models calculated parameters for In(III) adsorption with TP-207, TP-260 IRA-743 and 3D TP-260 adsorbent

Adsorbent	q_e exp (mg/g)	Pseudo first order kinetic model			Pseudo second order kinetic model		
		q_e , calc (mg/g)	k_1 (1/min)	R^2	q_e , calc (mg/g)	k_2 g/mg.min	R^2
TP-207	56,21	20,84	0,0034	0,4713	54,66	1.60E-03	0,9981
TP-260	56,18	20,90	0,0021	0,3293	50,00	6.03E-03	0,9971
IRA-743	38,99	33,75	0,0020	0,9176	40,32	1.81E-04	0,8146
3D TP-260	53,37	35,33	0,0310	0,9141	50,00	4,23E-03	0,9935

8.4 Initial concentration effect

The effect of the initial concentration of In(III) adsorption on four distinct adsorbents was investigated by maintaining all other parameters constant and varying just the Indium concentration in the solution. Figure 31-34 illustrates the influence of initial concentration on the removal efficiency and adsorption capacity.

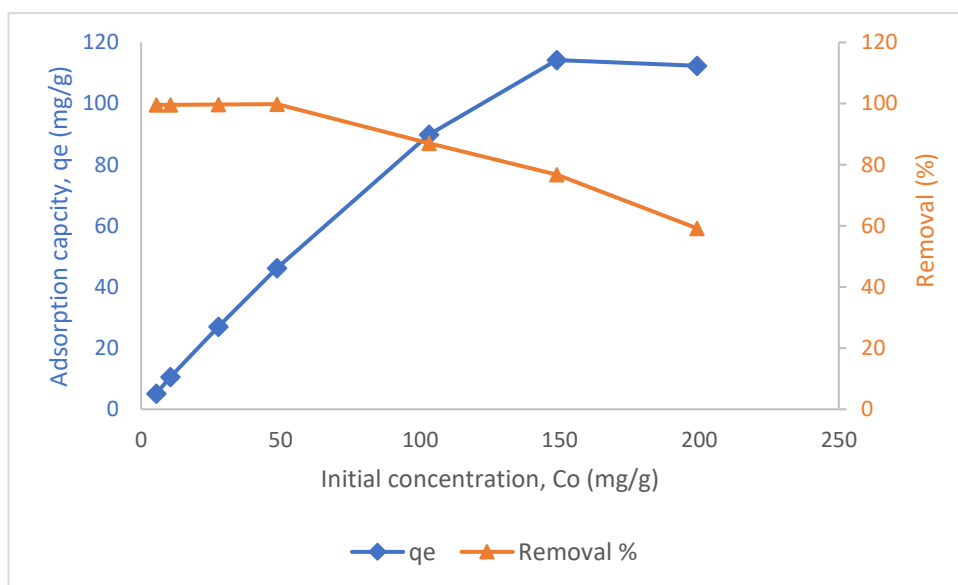


Figure 31 effect of initial concentration on In(III) adsorption by resin TP-207 at concentration range 5-200ppm, pH 3.5, contact time 12hr, shaking speed 500rpm and 25°C temperature.

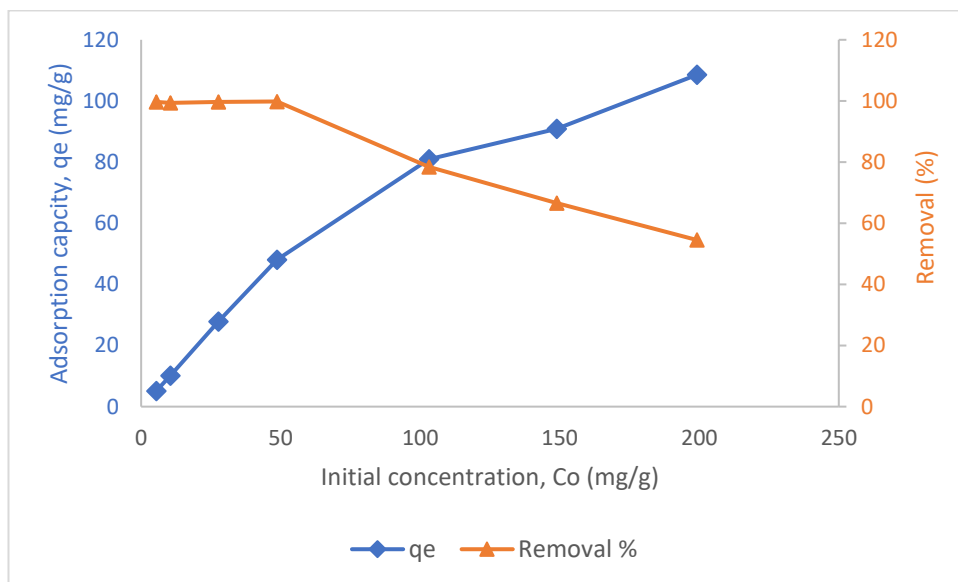


Figure 32 effect of initial concentration on In(III) adsorption by resin TP-260 at concentration range 5-200ppm, pH 3.5, contact time 12hr, shaking speed 500rpm and 25°C temperature.

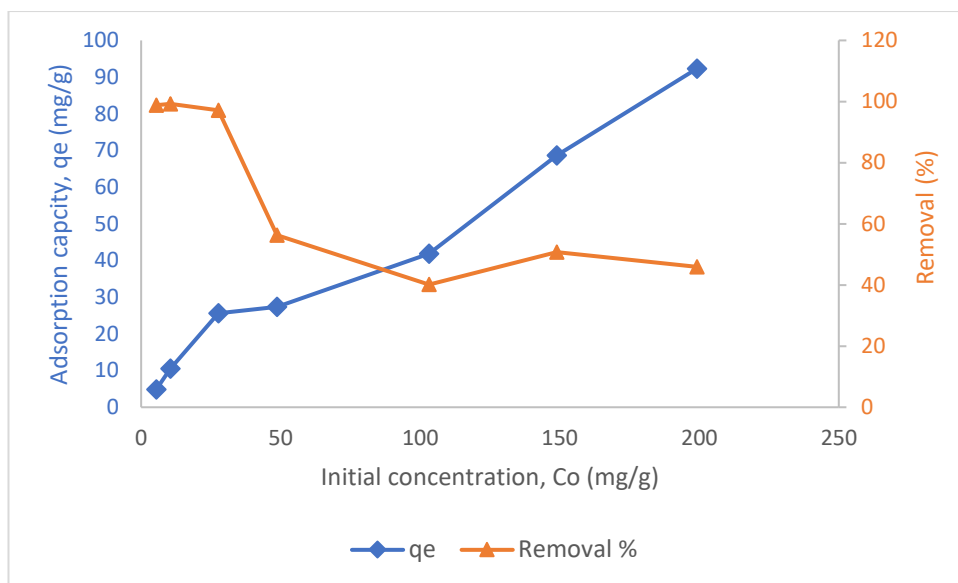


Figure 33 effect of initial concentration on In(III) adsorption by resin IRA-743 at concentration range 5-200ppm, pH 3.5, contact time 12hr, shaking speed 500rpm and 25°C temperature.

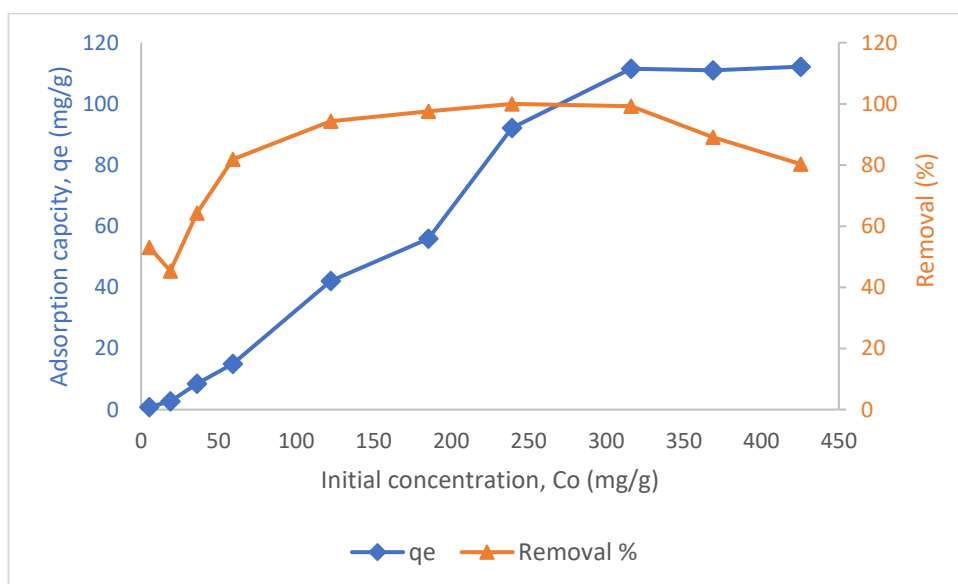


Figure 34 effect of initial concentration on In(III) adsorption by 3D printed TP-260 adsorbent at concentration range 5-425ppm, pH 3.5, contact time 6hr, shaking speed 500rpm and 25°C temperature.

All curves demonstrated that as adsorbent concentration increased, capacity increased while removal efficiency decreased that followed by (Kumar *et al.*, 2019) statement. While the adsorbed concentration is low in solution, the adsorbent surface area and active sites are significantly more than the amount adsorbed. Similarly, as the adsorbed concentration increases, the active sites are filled by adsorbing In(III) existing in the solution and the surface

area is covered, resulting in a scarcity of active sites for subsequent adsorption processes and a drop in removal efficiency (Z and G, 2003). In this situation, increased concentration was the driving force behind the adsorbent's increased adsorption capability. (Wang, Wang and Ma, 2010)

8.5 Adsorption Isotherms

The adsorption isotherms are widely used to deduce the mechanism of adsorption. Adsorption models are a collection of mathematical expressions that transform an experimental parameter to a standard equation (Srivastava, Ayachi and Mishra, 2001). The adsorption process is a physicochemical event that continues until an equilibrium condition is reached. Equilibrium states are defined as those in which the rate of adsorption and desorption are equal. The concentration of solute on the adsorbent surface q_e (mg/g) and the concentration of solute in solution C_e are used to characterize the equilibrium. There are various models constructed for adsorption processes, including the Langmuir and Freundlich isotherms, which are frequently used to characterize adsorption processes and provide data for batch adsorption process optimization (Cooney, 1999).

In isotherm modeling, the same operational parameter was employed as in the influence of initial concentration part.

8.5.1 Langmuir Isotherm

To establish the Langmuir isotherm model, the experimental data for In(III) adsorption equilibrium were fitted to the model using equation (11). Figure 35 was created by plotting experimental data in accordance with the model. The graphic depicts the linear model equation, and the R^2 value for each adsorbent indicates the model's quality. According to the R^2 value, the TP-207 adsorbent model fits better than the others with a value of 0.9946, the model for TP-260 is followed by and provides an R^2 value of 0.9104, and the IRA 743 adsorbent equilibrium data is less than the others (R^2 0.8576). The Langmuir isotherm represents the monolayer coverage of an adsorbent by adsorbed molecules. As the model R^2 value was considerable, it was predicted that the TP-207, TP-260, and IRA 743 adsorbents act via cation ion exchange to adsorb the In(III) on their surface. (M *et al.*, 2006)

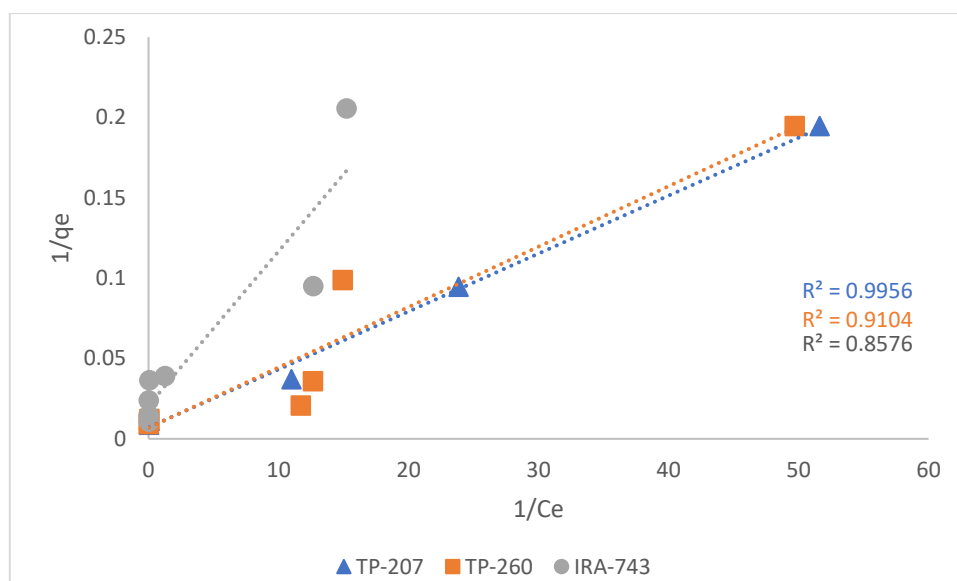


Figure 35 Langmuir isotherm model for TP-207, TP-260 and IRA-743 at concentration range 5-200ppm, pH 3.5, contact time 6hr, shaking speed 500rpm and 25°C temperatures.

However, the same data set was put to the Freundlich model to determine its applicability. Figure 36 displays the calculated value for each adsorbent parameter from the model.

Table 3 Langmuir and Freundlich isotherm model predicted parameter value

Adsorbent	Langmuir Isotherm			Freundlich Isotherm		
	qm (mg/g)	K_L	R^2	K_F	1/n	R^2
TP-207	138.88	2	0.9956	38.35	0.3046	0.7905
TP-260	144.92	1.92	0.9104	34.4	0.275	0.7347
IRA-743	48.3	2.16	0.8576	17.05	0.2925	0.8604

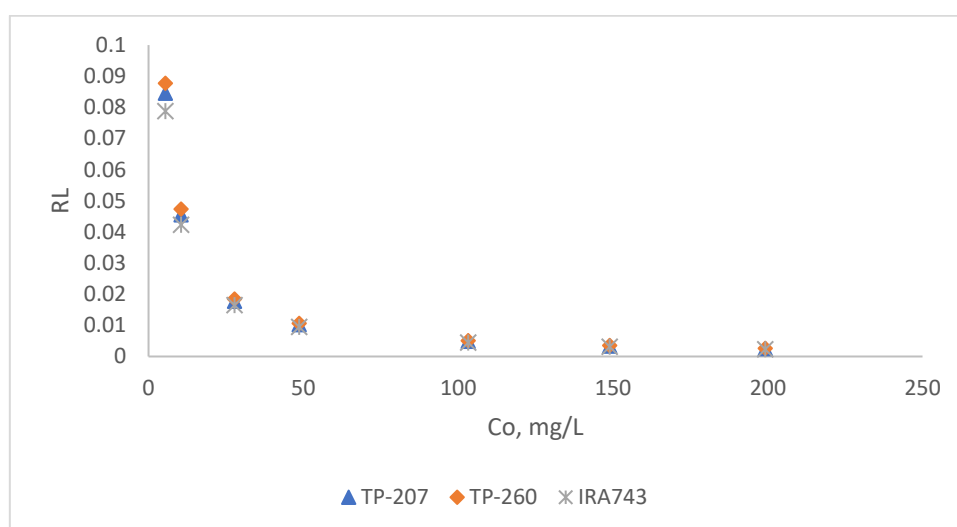


Figure 36 R_L vs concentration of In(III) plot

The separation factor R_L value is plotted against the initial concentration I_n (III). Figure 36 depicts, which confirms that all the data are in favorable condition for the Langmuir isotherm study.

8.5.2 Freundlich Isotherm

The experimental data for TP-207, TP-260, and IRA-743 were plotted using Freundlich isotherm linear equation (14), which resulted in the following Figure 37. The graph demonstrates that the adsorbent IRA743 has a higher R^2 value of 0.8604 while the other two had values less than 0.8, implying that the Freundlich model was not suited for those adsorbent adsorption processes. Although the R^2 value of the adsorbent IRA 743 model was more than that of the Langmuir isotherm model, the model projected value was not accurate. The expected value as calculated by the model is presented in Table 3. The Langmuir isotherm model can be applied to all three adsorbents. The 3D printed TP-260 did not adhere to any adsorption model. Additional research is required to fully understand the adsorption mechanism.

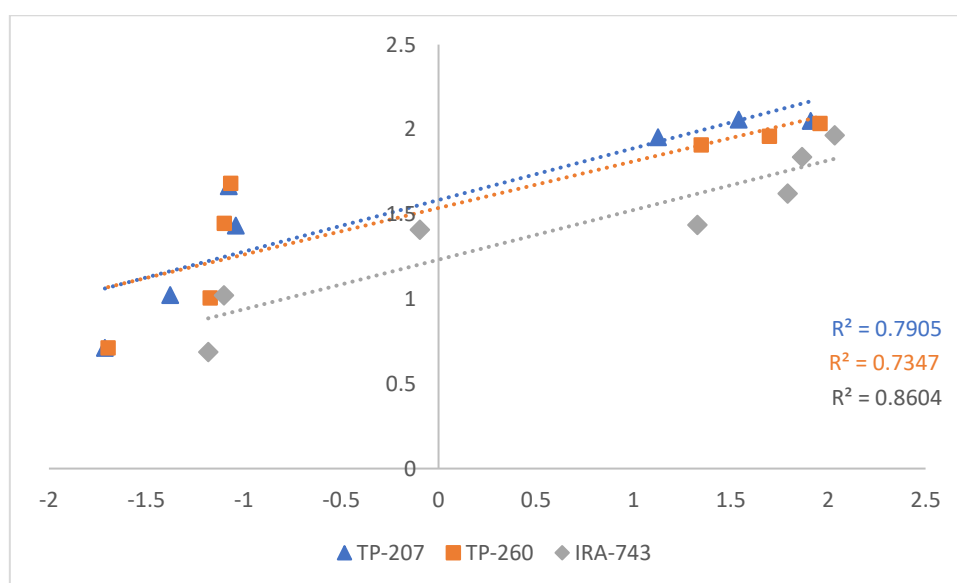


Figure 37 Freundlich isotherm model for TP-207, TP-260 and IRA-743 at concentration range 5-200ppm, pH 3.5, contact time 6hr, shaking speed 500rpm and 25°C temperatures

A comparative study data of indium adsorption shown in Table 4

Table 4 Comparative study table

Adsorbent	Operating parameter	Adsorption capacity, mg/g	Reference
In(III) ion and non-ion imprinted polymer	pH 3	47.3 and 31.1 respectively	(Li <i>et al.</i> , 2015)
Resin IDA	pH 4.52	235.5	(XIONG and YAO, 2008b)
CSIRs	pH 1.5, continuous flow, flow rate dependent adsorption capacity	26.2	(Yuan <i>et al.</i> , 2010)
Lewatiti TP-207	pH 0.8	55	(Lee and Lee, 2016)
Lewatiti TP-207	pH 3.5 batch mode	114	This work
Lewatit TP-260	pH 3.5 batch mode	108	This work
Amberlite IRA-743	pH 3.5 batch mode	92.32	This work
3D Printed TP-260	pH 3.5 batch mode	112	This work

8.6 Indium preconcentration and regeneration

Utilizing column adsorption techniques, Indium was preconcentrated from brine. Three adsorption batches were done using 500mL brine solution and HCL acid was employed as the eluent to recover In (III). Three consecutive batches were done using the same adsorbent. The table below depicts the Indium preconcentration data, with the first batch recovery yield of 0.978, the second batch recovery yield of 0.8651, and the third batch recovery yield being flawed. However, the 3D printed adsorbent showed better result for the first two batches, and the experiment was conducted only once, requiring more batch trials to optimize the column adsorption process parameters.

Table 5 In(III) preconcentration data

	Brine Solution volume (L)	In concentration in brine mg/L	Total In mass, (mg) present in solution	Eluent volume, (L)	ICP result ppm	In(III) recovered amount, (mg)	Recovery Yield
First batch	0,5	0,075285	0,0376425	0,0175	2,1039786	0,03681963	0,978139727
Second batch	0,5	0,075285	0,0376425	0,012	2,7138152	0,03256578	0,865133354
Third batch	0,5	0,075285	0,0376425	0,011	4,9282172	0,05421039	1,440137862

8.7 Adsorbent characterization

The SEM and FTIR analyses were used to describe the adsorbent, and the detailed results of those analyses are presented in the next subsection.

8.7.1 Scanning Electron Microscopy

Figure 38-41 illustrates the morphology of four different adsorbents. The left-hand picture depicts the adsorbent surface before the adsorption, while the right-hand figure depicts the In(III)-loaded adsorbent after adsorption. The figure illustrates the difference between a virgin adsorbent surface and a metal-loaded adsorbent surface. The presence of black particles on the TP-260 adsorbent and a white dot/spot on the remainder of the adsorbent could suggest the presence of In(III) on the adsorbent surface. EDS analysis is necessary for confirmation, which will be performed in subsequent study. While granular adsorbents had a smooth surface, 3D printed TP-260 had a porous surface, with irregular particle size and distribution.

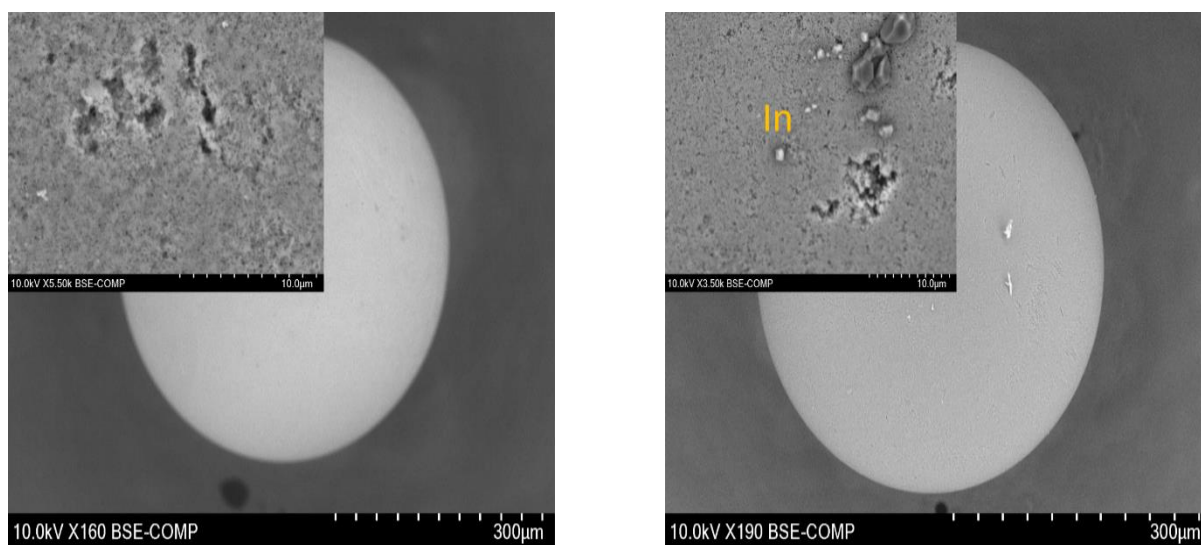


Figure 38 SEM image of TP-207 before (left) and after adsorption (right)

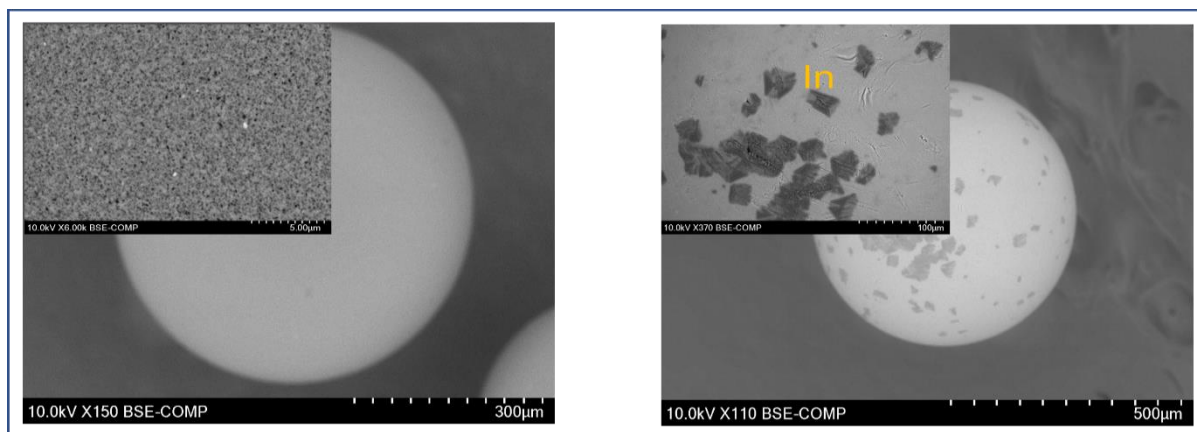


Figure 39 SEM image of TP-260 before (left) and after adsorption (right)

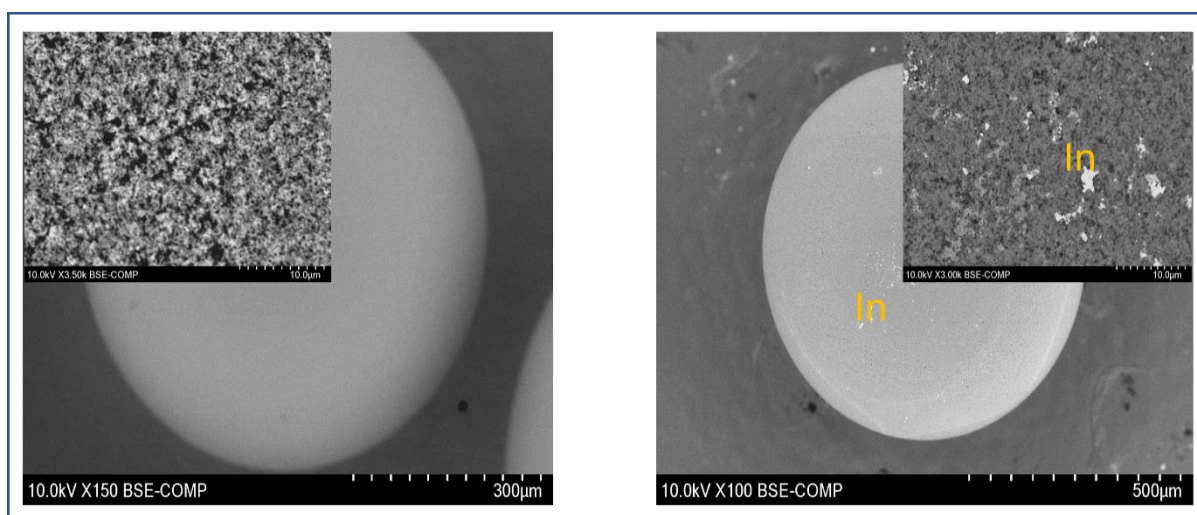


Figure 40 SEM image of IRA-743 before (left) and after adsorption (right)

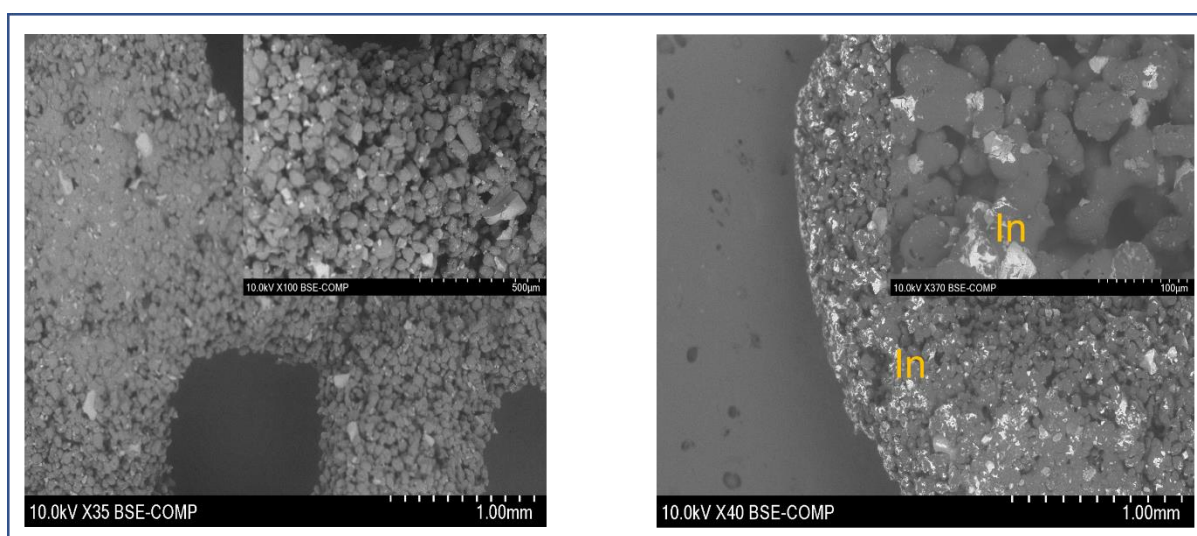


Figure 41 SEM image of 3D printed 3D TP-260 before (left) and after adsorption (right)

8.7.2 Fourier Transform Infrared Spectroscopy (FTIR) analysis

FTIR analysis was done on Lewatit TP-260, Nylon-12, and 3D printed TP-260, which is made up of 10% ion exchange resin and 90% nylon. The FTIR spectra of those compounds are shown in Figure 42. The spectra below explain the functional groups found in TP-260. A large peak appears in the figure at 3314 cm^{-1} , indicating the presence of O-H and N-H stretching bonds, which specifically indicate the sign of ion exchange. Peak 1655 cm^{-1} indicated the presence of the O-H water group during the ion exchange phase. A modest peak for asymmetric $-\text{CH}_2$ stretching observed at 2979 cm^{-1} . Carbon-carbon stretching (C=C) in right carbon emerged at 1467 cm^{-1} , whereas two peaks appeared at 710 cm^{-1} and 981 cm^{-1} , describing the vibration of deformation for the 1,4 dispersed benzene rings. (Kołodzyńska, Hubicki and Pasiieczna-Patkowska, 2009)

As a polyamide, nylon 12 is distinguished from other polymers by the presence of secondary amides, which assist to maintain the amide bond link between the N-H and C-N bonds (Smith, 2018). Stretching and bending are two types of vibrational effects that have been seen for the N-H bond, with the peak appearing in the range of 3370 to 3170 cm^{-1} . The presence of secondary amides in the compound was verified by the emergence of a peak in the range 1680 - 1630 cm^{-1} for C=O stretching, indicating the presence of secondary amides in the molecule. It is feasible for the in-plane vibration of N-H bending to occur as either an in-plane or an out-of-plane vibration; for secondary amide, the peak appeared for the in-plane vibration of N-H bending at 1570 - 1515 cm^{-1} and the peak appeared for the out-of-plane vibration at 1570 - 1515 cm^{-1} . The development of a peak at 724 cm^{-1} , which indicates the presence of the N-H bending vibration, helps to identify it. (Han, Cao and Gao, 2013)

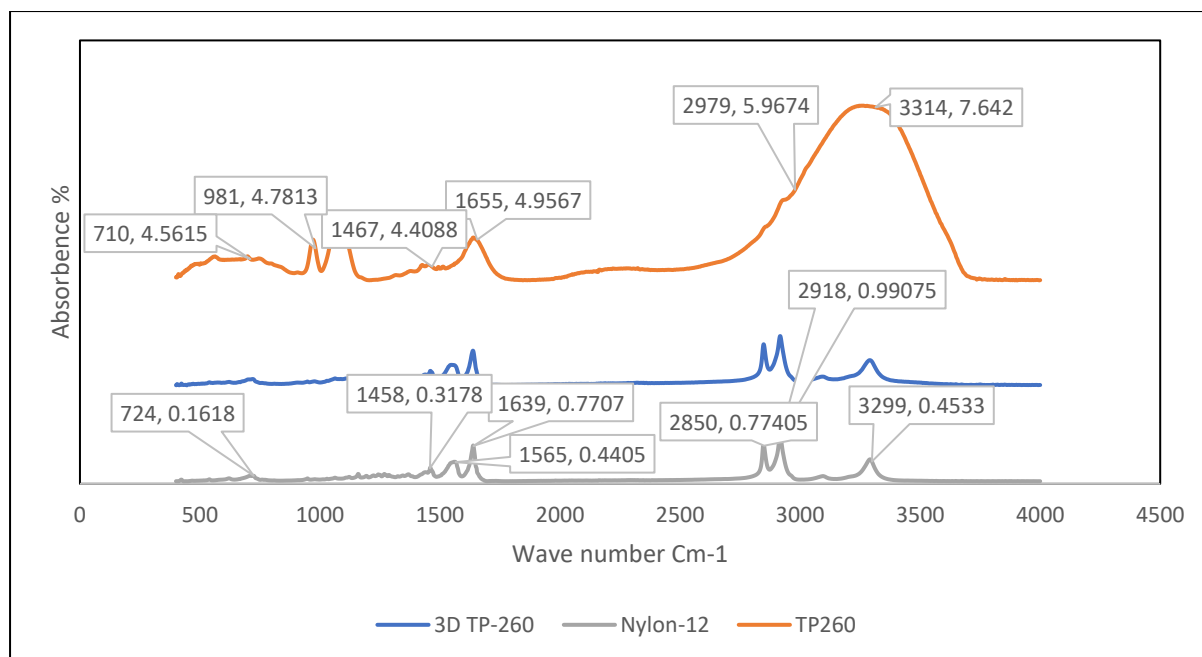


Figure 42 FTIR spectra TP-207, Nylon-12 and 3D TP-207

The TP-260 adsorbent, which was 3D printed, produced spectra that were like nylon 12. Due to the significant amount of nylon 12 present on the resin surface, as well as the absence of IR transmission through the sample, this may appear to be the case. It is necessary to detect functional groups on 3D printed structures using microscopic FTIR. This may be conducted in future work.

9. Conclusions

The goal of this thesis study was to develop technologies for recovering Indium from seawater brine solutions via adsorption. The entire study can be divided into three parts: first, three commercial resins were used in regular form to observe adsorptive behavior for Indium; second, the experimental analysis data were evaluated, and suitable Indium adsorption functional resin figure out and taken resin for AM manufacturing process; in the last phase, an additively produced adsorbent was subjected to batch adsorption using Indium standard solution and column adsorption tests in order to accomplish Indium preconcentrating using brine solution.

This study was employed to the following commercial resins: Lewatit TP-207 iminodiacetic acid-based cation exchange resin, Lewatit TP-260 phosphonic acid-based cation exchange resin, and Amberlite IRA-743 chelating cation exchange resin. In the kinetic behavior analysis, TP-260 had a higher adsorption capacity for a shorter period than the other two resins, with a maximum adsorption capacity of 56 mg/g at 240 minutes. Based on this finding, the TP-260 resin was chosen for 3D printed adsorbent manufacture, with 10% resin and 90% nylon 12 employed as raw materials. The batch adsorption experiment was carried out utilizing 3D printed TP-260 and yielded about the same adsorption capacity as general formed resin TP-260. At 120 minutes, the maximum adsorption capacity of 3D printed TP 260 was 52mg/g. This finding is quite surprising, because the results could worsen owing to the ion exchange resin active site capping by the nylon 12 materials because there is no strong evidence that nylon 12 materials have functionality for Indium adsorption.

The kinetic analysis revealed that all the adsorbents used in this study followed pseudo second order reaction kinetic, which was assessed using the R2 value and model predicted value variation. Although the adsorbent IRA-743 had a greater value for the pseudo first order kinetic, the second order model projected value was more accurate than the pseudo first order kinetic.

On the equilibrium experimental data of each adsorbent, the Langmuir and Freundlich isotherm models were used, and it seems that three ion exchange resins followed the Langmuir isotherm, indicating monolayer adsorption of In(III) on the adsorbent surface. The experimental data

appropriateness for those three adsorbents was also verified, and all data were determined to be beneficial for Indium adsorption. The 3D printed TP-260, on the other hand, did not adhere to any isotherm model. It may occur as a result of the adsorbent's heterogeneous surface and multi-layer adsorption. More research is needed to determine the true cause of this.

To preconcentrate Indium from brine solution, column-based adsorption was used. In this experiment, the first two batches provided significant Indium recovery yield (1st batch: 0,978 and 2nd batch: 0,8651), whereas the third batch experiment was reported as flawed. Further trials are required to optimize process parameters, eluent acid concentration, and the structure of the 3D printed adsorbent.

A few recommendations for future work are enlisted below:

- Indium selective adsorbent has not been tested yet. That is required to be done in the future.
- EDS analysis is required to confirm the presence of Indium on the adsorbent surface.
- Zeta potential analysis may be used to characterize the adsorbent.
- Optimization of column adsorption parameters and 3D-printed adsorbent design
- Characterize the column adsorption mechanism.
- Due to a lack of IR rays passing through the sample in conventional FTIR instruments, the microscopic FTIR analysis necessary to identify the surface functional group as a 3D printed component did not produce a meaningful result for the 3D manufactured adsorbent.

10. References

- Akama, Y., Suzuki, S. and Monobe, Y. (2016) “STUDY ON THE ADSORPTION AND SELECTIVE SEPARATION OF INDIUM FROM ZINC WITH CHELATING CELLULOSE,” *CELLULOSE CHEMISTRY AND TECHNOLOGY Cellulose Chem. Technol.*, 50(1), pp. 147–152.
- Alfantazi, A.M.; Moskalyk, R.R. (2003) “Processing of Indium: a review,” *Mineral Engineering*, 16(8), pp. 687–694. doi:10.1016/S0892-6875(03)00168-7.
- Alguacil, F.J. *et al.* (2016) “Sorption of indium (III) onto carbon nanotubes,” *Ecotoxicology and Environmental Safety*, 130. doi:10.1016/j.ecoenv.2016.04.008.
- Amakawa, H., Alibo, D.S. and Nozaki, Y. (1996) “Indium concentration in Pacific seawater,” *Geophysical Research Letters*, 23(18), pp. 2473–2476. doi:10.1029/96GL02300.
- Argenta, A.B. *et al.* (2017) “Supercritical CO₂ extraction of indium present in liquid crystal displays from discarded cell phones using organic acids,” *The Journal of Supercritical Fluids*, 120, pp. 95–101. doi:10.1016/J.SUPFLU.2016.10.014.
- Assefi, M. *et al.* (2018a) “Selective recovery of indium from scrap LCD panels using macroporous resins,” *Journal of Cleaner Production*, 180, pp. 814–822. doi:10.1016/J.JCLEPRO.2018.01.165.
- Assefi, M. *et al.* (2018b) “Selective recovery of indium from scrap LCD panels using macroporous resins,” *Journal of Cleaner Production*, 180, pp. 814–822. doi:10.1016/J.JCLEPRO.2018.01.165.
- B, C. *et al.* (2011) “Synthesis of hierarchical Ni(OH)₂ and NiO nanosheets and their adsorption kinetics and isotherms to Congo red in water,” *Journal of hazardous materials*, 185(2–3), pp. 889–897. doi:10.1016/J.JHAZMAT.2010.09.104.
- B, S. *et al.* (2016a) “Beneficiation and recovery of indium from liquid-crystal-display glass by hydrometallurgy,” *Waste management (New York, N.Y.)*, 57, pp. 207–214. doi:10.1016/J.WASMAN.2016.02.019.
- B, S. *et al.* (2016b) “Beneficiation and recovery of indium from liquid-crystal-display glass by hydrometallurgy,” *Waste management (New York, N.Y.)*, 57, pp. 207–214. doi:10.1016/J.WASMAN.2016.02.019.
- Balla, V.K., Bose, S. and Bandyopadhyay, A. (2008) “Processing of Bulk Alumina Ceramics Using Laser Engineered Net Shaping,” *International Journal of Applied Ceramic Technology*, 5(3), pp. 234–242. doi:10.1111/J.1744-7402.2008.02202.X.
- Binder Jetting | Additive Manufacturing Research Group | Loughborough University* (no date). Available at: <https://www.lboro.ac.uk/research/amrg/about/the7categoriesofadditivemanufacturing/binderjetting/> (Accessed: August 27, 2021).

- Bolt, G.H. and van Olphen, H. (1985) "The Surface Chemistry of Soils," *Clays and Clay Minerals* 1985 33:4, 33(4), pp. 367–367. doi:10.1346/CCMN.1985.0330415.
- Caulfield, B., McHugh, P.E. and Lohfeld, S. (2007) "Dependence of mechanical properties of polyamide components on build parameters in the SLS process," *Journal of Materials Processing Technology*, 182(1–3), pp. 477–488. doi:10.1016/J.JMATPROTEC.2006.09.007.
- Chang, J. *et al.* (2016) "Separation of indium from iron in a rotating packed bed contactor using Di-2-ethylhexylphosphoric acid," *Separation and Purification Technology*, 164, pp. 12–18. doi:10.1016/J.SEPPUR.2016.03.017.
- Chow, T.J. and Snyder, C.B. (1969) "Indium content of sea water," *Earth and Planetary Science Letters*, 7(3), pp. 221–223. doi:10.1016/0012-821X(69)90054-5.
- Cooney, D.O. (1999) "Adsorption design for wastewater treatment," p. 190.
- Criales, L.E. *et al.* (2017) "Laser powder bed fusion of nickel alloy 625: Experimental investigations of effects of process parameters on melt pool size and shape with spatter analysis," *International Journal of Machine Tools and Manufacture*, 121, pp. 22–36. doi:10.1016/J.IJMACHTOOLS.2017.03.004.
- Crundwell, F.K. (1988) "Effect of iron impurity in zinc sulfide concentrates on the rate of dissolution," *AIChE Journal*, 34(7), pp. 1128–1134. doi:10.1002/AIC.690340709.
- D, F. *et al.* (2015) "Materials recovery from waste liquid crystal displays: A focus on indium," *Waste management (New York, N.Y.)*, 45, pp. 325–333. doi:10.1016/J.WASMAN.2015.07.043.
- Deckers, J., Vleugels, J. and Kruth, J.P. (2014) "Additive manufacturing of ceramics: A review," *Journal of Ceramic Science and Technology*, 5(4), pp. 245–260. doi:10.4416/JCST2014-00032.
- Deferm, C. *et al.* (2017) "Speciation of indium(iii) chloro complexes in the solvent extraction process from chloride aqueous solutions to ionic liquids," *Dalton Transactions*, 46(13). doi:10.1039/c7dt00618g.
- Downs, A.J. (1993) *Chemistry of Aluminium, Gallium, Indium and Thallium*. First Edit.
- F, F. *et al.* (2017) "Separation and recovery of glass, plastic and indium from spent LCD panels," *Waste management (New York, N.Y.)*, 60, pp. 569–581. doi:10.1016/J.WASMAN.2016.12.030.
- Feng, L., Wang, Y. and Wei, Q. (2019) "PA12 Powder Recycled from SLS for FDM," *Polymers* 2019, Vol. 11, Page 727, 11(4), p. 727. doi:10.3390/POLYM11040727.
- Filippou, D. and Demopoulos, G.P. (1997) "Steady-state modeling of zinc-ferrite hot-acid leaching," *Metallurgical and Materials Transactions B* 1997 28:4, 28(4), pp. 701–711. doi:10.1007/S11663-997-0044-0.
- Foo, K.Y. and Hameed, B.H. (2010) "Insights into the modeling of adsorption isotherm systems," *Chemical Engineering Journal*, 156(1), pp. 2–10. doi:10.1016/J.CEJ.2009.09.013.

Fortes, M. C.B., Martins, A.H. and Benedetto, J.S. (2007) "Selective separation of indium by iminodiacetic acid chelating resin," *Brazilian Journal of Chemical Engineering*, 24(2), pp. 287–292. doi:10.1590/S0104-66322007000200013.

Fortes, M. C. B., Martins, A.H. and Benedetto, J.S. (2007) "Selective separation of indium by iminodiacetic acid chelating resin," *Brazilian Journal of Chemical Engineering*, 24(2), pp. 287–292. doi:10.1590/S0104-66322007000200013.

French, S.J. (1934) "A story of indium," *Journal of Chemical Education*, 11(5), p. 270. doi:10.1021/ed011p270.

Frenzel, Max; Mikolajczak, Claire; Reuter, Markus A.; Gutzmer, J. (2017) "Quantifying the relative availability of high-tech by-product metals – The cases of gallium, germanium and indium," *Resource Policy*, 52, pp. 327–335. doi:10.1016/j.resourpol.2017.04.008.

Frenzel, Max; Tolosana-Delgado, Raimon; Gutzmer, J. (2015) "Assessing the supply potential of high-tech metals – A general method", *Resource Policy*, 46(part 2), pp. 45–58. doi:10.1016/j.resourpol.2015.08.002.

Ghoreishi, S.M., Ansari, K. and Ghaziaskar, H.S. (2012) "Supercritical extraction of toxic heavy metals from aqueous waste via Cyanex 301 as chelating agent," *The Journal of Supercritical Fluids*, 72, pp. 288–297. doi:10.1016/J.SUPFLU.2012.10.003.

Gibson, I., Rosen, D.W. and Stucker, B. (2010) "Additive manufacturing technologies: Rapid prototyping to direct digital manufacturing," *Additive Manufacturing Technologies: Rapid Prototyping to Direct Digital Manufacturing*, pp. 1–459. doi:10.1007/978-1-4419-1120-9.

Giles, C.H., Smith, D. and Huitson, A. (1974) "A general treatment and classification of the solute adsorption isotherm. I. Theoretical," *Journal of Colloid and Interface Science*, 47(3), pp. 755–765. doi:10.1016/0021-9797(74)90252-5.

Greenwood, N.N.; Earnshaw, A. (1997) *Chemistry of the Elements*. Second Edi. Pergamon Press plc.

Grimes, S.M., Yasri, N.G. and Chaudhary, A.J. (2017) "Recovery of critical metals from dilute leach solutions – Separation of indium from tin and lead," *Inorganica Chimica Acta*, 461, pp. 161–166. doi:10.1016/J.ICA.2017.02.002.

H, Y., M, T. and Y, T. (1999) "Production of organic acids and amino acids from fish meat by sub-critical water hydrolysis," *Biotechnology progress*, 15(6), pp. 1090–1094. doi:10.1021/BP9900920.

Han, J., Cao, Z. and Gao, W. (2013) "Remarkable sorption properties of polyamide 12 microspheres for a broad-spectrum antibacterial (triclosan) in water," *Journal of Materials Chemistry A*, 1(16), pp. 4941–4944. doi:10.1039/C3TA00090G.

Hanna, O. T., Sandall, O.C. (1995) "Computational Method in Chemical Engineering," *Englewood Cliffs, NJ: Prentice-Hall International*, pp. 127–130.

Hasegawa, H. *et al.* (2013) "Selective recovery of indium from the etching waste solution of the flat-panel display fabrication process," *Microchemical Journal*, 110, pp. 133–139. doi:10.1016/J.MICROC.2013.03.005.

- Haynes, W.M, Lide, D.R. (2010) *CRC Handbook of Chemistry and Physics: A ready reference book of Chemical and Physical Data*.
- Hinz, C. (2001) "Description of sorption data with isotherm equations," *Geoderma*, 99(3–4), pp. 225–243. doi:10.1016/S0016-7061(00)00071-9.
- Ho, H.C.H., Gibson, I. and Cheung, W.L. (1999) "Effects of energy density on morphology and properties of selective laser sintered polycarbonate," *Journal of Materials Processing Technology*, 89–90, pp. 204–210. doi:10.1016/S0924-0136(99)00007-2.
- Ho, Y.S. and McKay, G. (1999) "Pseudo-second order model for sorption processes," *Process Biochemistry*, 34(5), pp. 451–465. doi:10.1016/S0032-9592(98)00112-5.
- Hofland, E.C., Baran, I. and Wismeijer, D.A. (2017) "Correlation of Process Parameters with Mechanical Properties of Laser Sintered PA12 Parts," *Advances in Materials Science and Engineering*, 2017. doi:10.1155/2017/4953173.
- Hsieh, S.-J., Chen, C.-C. and Say, W.C. (2009) "Process for recovery of indium from ITO scraps and metallurgic microstructures," *Materials Science & Engineering B*, 1–3(158), pp. 82–87. doi:10.1016/J.MSEB.2009.01.019.
- J, L. *et al.* (2009) "Recovery of valuable materials from waste liquid crystal display panel," *Waste management (New York, N.Y.)*, 29(7), pp. 2033–2039. doi:10.1016/J.WASMAN.2008.12.013.
- Jeon, C., Cha, J.H. and Choi, J.Y. (2015) "Adsorption and recovery characteristics of phosphorylated sawdust bead for indium(III) in industrial wastewater," *Journal of Industrial and Engineering Chemistry*, 27, pp. 201–206. doi:10.1016/J.JIEC.2014.12.036.
- Jiang, J., Liang, D. and Zhong, Q. (2011) "Precipitation of indium using sodium tripolyphosphate," *Hydrometallurgy*, 106(3–4), pp. 165–169. doi:10.1016/J.HYDROMET.2010.12.009.
- Kapoor, A. and Yang, R.T. (1989) "Correlation of equilibrium adsorption data of condensable vapours on porous adsorbents," *Gas Separation & Purification*, 3(4), pp. 187–192. doi:10.1016/0950-4214(89)80004-0.
- Kato, T. *et al.* (2013) "Separation and concentration of indium from a liquid crystal display via homogeneous liquid–liquid extraction," *Hydrometallurgy, Complete*(137), pp. 148–155. doi:10.1016/J.HYDROMET.2013.06.004.
- Kaukinen, A., Sc, D. and Virolainen, S. (no date) "Ion exchange in hydrometallurgical recycling of Li-ion battery metals: production of Li-Ni-Co mixture Examiners: Professor Tuomo Sainio."
- Kołodziejka, D., Hubicki, Z. and Pasieczna-Patkowska, S. (2009) "FT-ir/pas studies of cu(II)-EDTA complexes sorption on the chelating ion exchangers," *Acta Physica Polonica A*, 116(3), pp. 340–343. doi:10.12693/APHYSPOLA.116.340.
- Kumar, M. *et al.* (2019) "Valorization of coal fired-fly ash for potential heavy metal removal from the single and multi-contaminated system," *Heliyon*, 5(10), p. e02562. doi:10.1016/J.HELİYON.2019.E02562.

- Kumar, S. (2020) "Introduction of Additive Manufacturing Processes," *Additive Manufacturing Processes*, pp. 1–19. doi:10.1007/978-3-030-45089-2_1.
- Kundu, S. and Gupta, A.K. (2006) "Arsenic adsorption onto iron oxide-coated cement (IOCC): Regression analysis of equilibrium data with several isotherm models and their optimization," *Chemical Engineering Journal*, 122(1–2), pp. 93–106. doi:10.1016/J.CEJ.2006.06.002.
- Lahtinen, E. *et al.* (2017) "Selective Recovery of Gold from Electronic Waste Using 3D-Printed Scavenger," *ACS Omega*, 2(10), pp. 7299–7304. doi:10.1021/acsomega.7b01215.
- Lahtinen, E. *et al.* (2018) "Porous 3D Printed Scavenger Filters for Selective Recovery of Precious Metals from Electronic Waste," *Advanced Sustainable Systems*, 2(10). doi:10.1002/adsu.201800048.
- Lahtinen, E. *et al.* (2019) "Selective Laser Sintering of Metal-Organic Frameworks: Production of Highly Porous Filters by 3D Printing onto a Polymeric Matrix," *ChemPlusChem*, 84(2), pp. 222–225. doi:10.1002/cplu.201900081.
- Langmuir, I. (2002) "THE ADSORPTION OF GASES ON PLANE SURFACES OF GLASS, MICA AND PLATINUM.," *Journal of the American Chemical Society*, 40(9), pp. 1361–1403. doi:10.1021/JA02242A004.
- Lee, S.K. and Lee, U.H. (2016) "Adsorption and desorption property of iminodiacetate resin (Lewatit® TP207) for indium recovery," *Journal of Industrial and Engineering Chemistry*, 40, pp. 23–25. doi:10.1016/J.JIEC.2016.05.016.
- Lewatit-Lenntech (no date) "Lewatit-MonoPlus-TP-260-Resin-Lenntech."
- Li, C. *et al.* (2010) "Oxidative pressure leaching of sphalerite concentrate with high indium and iron content in sulfuric acid medium," *Hydrometallurgy*, 102(1–4), pp. 91–94. doi:10.1016/J.HYDROMET.2010.01.009.
- Li, F. *et al.* (2018) "High efficient separation of U(VI) and Th(IV) from rare earth elements in strong acidic solution by selective sorption on phenanthroline diamide functionalized graphene oxide," *Chemical Engineering Journal*, 332. doi:10.1016/j.cej.2017.09.038.
- Li, H. *et al.* (2012) "Adsorption behavior of indium(III) on modified solvent impregnated resins (MSIRs) containing sec-octylphenoxy acetic acid," *Hydrometallurgy*, 121–124, pp. 60–67. doi:10.1016/J.HYDROMET.2012.04.005.
- Li, M. *et al.* (2018) "A novel In(III) ion-imprinted polymer (IIP) for selective extraction of In(III) ions from aqueous solutions," *Hydrometallurgy*, 176. doi:10.1016/j.hydromet.2018.02.006.
- Li, Min *et al.* (2015) "Synthesis and application of a surface-grafted In (III) ion-imprinted polymer for selective separation and pre-concentration of indium (III) ion from aqueous solution," *Hydrometallurgy*, Complete(154), pp. 63–71. doi:10.1016/J.HYDROMET.2015.03.011.

- Li, R. Di *et al.* (2014a) “Recovery of indium by acid leaching waste ITO target based on neural network,” *Transactions of Nonferrous Metals Society of China*, 24(1), pp. 257–262. doi:10.1016/S1003-6326(14)63055-7.
- Li, R. Di *et al.* (2014b) “Recovery of indium by acid leaching waste ITO target based on neural network,” *Transactions of Nonferrous Metals Society of China*, 24(1), pp. 257–262. doi:10.1016/S1003-6326(14)63055-7.
- Li, X.-H. *et al.* (2010) “Indium recovery from zinc oxide flue dust by oxidative pressure leaching,” *Trans. Nonferrous Met. Soc. China*, 20, pp. 141–145.
- Li, Y. *et al.* (2011) “Recovery of indium from used indium–tin oxide (ITO) targets,” *Hydrometallurgy*, 105(3–4), pp. 207–212. doi:10.1016/J.HYDROMET.2010.09.006.
- Liu, L. *et al.* (2019) “Application of Nanotechnology in the Removal of Heavy Metal From Water,” *Nanomaterials for the Removal of Pollutants and Resource Reutilization*, pp. 83–147. doi:10.1016/B978-0-12-814837-2.00004-4.
- Lokanc, M., Eggert, R. and Redlinger, M. (2015) “The Availability of Indium: The Present, Medium Term, and Long Term.” doi:10.2172/1327212.
- M, N. *et al.* (2006) “Sorption of lead from aqueous solution by chemically modified carbon adsorbents,” *Journal of hazardous materials*, 138(3), pp. 604–613. doi:10.1016/J.JHAZMAT.2006.05.098.
- Malek A., Farooq, S. (1996) “Comparison of isotherm models for hydrocarbon on activated carbon,” *The American Institute of Chemical Engineers Journal*, 42(11), pp. 3191–3201.
- Mane, V.S., Deo Mall, I. and Chandra Srivastava, V. (2007) “Kinetic and equilibrium isotherm studies for the adsorptive removal of Brilliant Green dye from aqueous solution by rice husk ash,” *Journal of Environmental Management*, 84(4), pp. 390–400. doi:10.1016/J.JENVMAN.2006.06.024.
- Marquardt, D.W. (2006) “An Algorithm for Least-Squares Estimation of Nonlinear Parameters,” <http://dx.doi.org/10.1137/0111030>, 11(2), pp. 431–441. doi:10.1137/0111030.
- Material Extrusion | Additive Manufacturing Research Group | Loughborough University* (no date). Available at: <https://www.lboro.ac.uk/research/amrg/about/the7categoriesofadditivemanufacturing/materialextrusion/> (Accessed: August 27, 2021).
- MATTHEWS, A.D. and RILEY, J.P. (1970) “Occurrence of Indium in Seawater and some Marine Sediments,” *Nature 1970* 225:5239, 225(5239), pp. 1242–1242. doi:10.1038/2251242a0.
- Myers, R.H. (1990) “Classical and Modern Regression with Applications,” *PWS-KENT*, 29(4), pp. 691–693.
- Ng, J.C.Y., Cheung, W.H. and McKay, G. (2002) “Equilibrium Studies of the Sorption of Cu(II) Ions onto Chitosan,” *Journal of Colloid and Interface Science*, 255(1), pp. 64–74. doi:10.1006/JCIS.2002.8664.

Ng, J.C.Y., Cheung, W.H. and McKay, G. (2003) "Equilibrium studies for the sorption of lead from effluents using chitosan," *Chemosphere*, 52(6), pp. 1021–1030. doi:10.1016/S0045-6535(03)00223-6.

Paiva, A.P. (2006) "RECOVERY OF INDIUM FROM AQUEOUS SOLUTIONS BY SOLVENT EXTRACTION," *Separation Science and Technology*, 36(7), pp. 1395–1419. doi:10.1081/SS-100103878.

Petrucci, R.H. (2007) *General Chemistry: Principles and Modern Applications- Principle of Extractive Metallurgy*. 9th editio. Prentice Hall: Pearson.

Plazinski, W., Rudzinski, W. and Plazinska, A. (2009) "Theoretical models of sorption kinetics including a surface reaction mechanism: A review," *Advances in Colloid and Interface Science*, 152(1–2), pp. 2–13. doi:10.1016/J.CIS.2009.07.009.

Pradhan, D., Panda, S. and Sukla, L.B. (2017) "Recent advances in indium metallurgy: A review," <https://doi.org/10.1080/08827508.2017.1399887>, 39(3), pp. 167–180. doi:10.1080/08827508.2017.1399887.

Ben Redwood and Filemon Schöffner (2017) *The 3D Printing Handbook: Technologies, design and applications*. Coers & Roest.

Ren, S. and Galjaard, S. (2015) "Topology Optimisation for Steel Structural Design with Additive Manufacturing," *Modelling Behaviour*, pp. 35–44. doi:10.1007/978-3-319-24208-8_3.

Repo, E., Warchoń, J.K. and Sillanpää, M. (2017) "Metal recovery and preconcentration by aminopolycarboxylic acid modified silica surfaces," *Journal of Sustainable Development of Energy, Water and Environment Systems*, 5(1), pp. 89–100. doi:10.13044/J.SDEWES.D5.0135.

Robati, D. (2013) "Pseudo-second-order kinetic equations for modeling adsorption systems for removal of lead ions using multi-walled carbon nanotube," *Journal of Nanostructure in Chemistry 2013 3:1*, 3(1), pp. 1–6. doi:10.1186/2193-8865-3-55.

Rocchetti, L. *et al.* (2015) "Cross-current leaching of indium from end-of-life LCD panels," *Waste Management*, 42, pp. 180–187. doi:10.1016/J.WASMAN.2015.04.035.

Rocchetti, L., Amato, A. and Beolchini, F. (2016) "Recovery of indium from liquid crystal displays," *Journal of Cleaner Production*, 116, pp. 299–305. doi:10.1016/J.JCLEPRO.2015.12.080.

Roschli, A. *et al.* (2019) "Designing for Big Area Additive Manufacturing," *Additive Manufacturing*, 25, pp. 275–285. doi:10.1016/J.ADDMA.2018.11.006.

Ruan, J., Guo, Y. and Qiao, Q. (2012) "Recovery of Indium from Scrap TFT-LCDs by Solvent Extraction," *Procedia Environmental Sciences*, 16, pp. 545–551. doi:10.1016/J.PROENV.2012.10.075.

Sachs, E.M. *et al.* (1993) "Three-dimensional printing techniques," 677(447), p. 55.

Sasaki, Y., Oshima, T. and Baba, Y. (2017) “Mutual separation of indium(III), gallium(III) and zinc(II) with alkylated aminophosphonic acids with different basicities of amine moiety,” *Separation and Purification Technology*, 173. doi:10.1016/j.seppur.2016.08.033.

Sawai, H. *et al.* (2015) “Selective recovery of indium from lead-smelting dust,” *Chemical Engineering Journal*, 277, pp. 219–228. doi:10.1016/J.CEJ.2015.04.112.

Schaeffer, N., Grimes, S.M. and Cheeseman, C.R. (2017) “Use of extraction chromatography in the recycling of critical metals from thin film leach solutions,” *Inorganica Chimica Acta*, 457, pp. 53–58. doi:10.1016/J.ICA.2016.11.020.

Sekhararaoogulipalli, C.H., Prasad and Wasewar (2011) “BATCHSTUDY,EQUILIBRIUMANDKINETICSSOFFFF ADSORPTIONOFFSELENIUMMUSINGGRICEEHUSKKASHH(RHA)),” 55(6), p. 5866.

Setiawan, H., Sakamoto, M. and Shiratori, Y. (no date) “IOP Conference Series: Earth and Environmental Science Development of ion-exchange properties of bamboo charcoal modified with concentrated nitric acid You may also like N-Doped Biochar as H₂ s Adsorbent for the Biogas-Fueled SOFC,” *IOP Conf. Ser.: Earth Environ. Sci.*, 82, p. 12002. doi:10.1088/1755-1315/82/1/012002.

Sheet Lamination | Additive Manufacturing Research Group | Loughborough University (no date). Available at: <https://www.lboro.ac.uk/research/amrg/about/the7categoriesofadditivemanufacturing/sheetlamination/> (Accessed: August 28, 2021).

Silveira, A.V.M. *et al.* (2015) “Recovery of indium from LCD screens of discarded cell phones,” *Waste Management*, 45, pp. 334–342. doi:10.1016/J.WASMAN.2015.04.007.

Sing, S.L. *et al.* (2020) “3D printing of metals in rapid prototyping of biomaterials: Techniques in additive manufacturing,” *Rapid Prototyping of Biomaterials: Techniques in Additive Manufacturing*, pp. 17–40. doi:10.1016/B978-0-08-102663-2.00002-2.

Sips, R. (2004) “On the Structure of a Catalyst Surface,” *The Journal of Chemical Physics*, 16(5), p. 490. doi:10.1063/1.1746922.

Sireesha, M. *et al.* (2018) “A review on additive manufacturing and its way into the oil and gas industry,” *RSC Advances*, 8(40), pp. 22460–22468. doi:10.1039/C8RA03194K.

Smith, B. (2018) “Infrared Spectral Interpretation : A Systematic Approach,” *Infrared Spectral Interpretation* [Preprint]. doi:10.1201/9780203750841.

Smith, J.A. and Galan, Adina. (2002) “Sorption of Nonionic Organic Contaminants to Single and Dual Organic Cation Bentonites from Water,” *Environmental Science and Technology*, 29(3), pp. 685–692. doi:10.1021/ES00003A016.

Soheila Karimi-Lotfabad, †, Michael A. Pickard, ‡ and and Murray R. Gray*, † (1996) “Reactions of Polynuclear Aromatic Hydrocarbons on Soil,” *Environmental Science and Technology*, 30(4), pp. 1145–1151. doi:10.1021/ES950365X.

- Srivastava, R.K., Ayachi, A.K. and Mishra, M. (2001) "Removal of chromium (VI) by utilization of bidi leaves," *Pollution Research*, 20, pp. 639–643.
- Tanhaei, B. *et al.* (2015) "Preparation and characterization of a novel chitosan/Al₂O₃/magnetite nanoparticles composite adsorbent for kinetic, thermodynamic and isotherm studies of Methyl Orange adsorption," *Chemical Engineering Journal*, 259, pp. 1–10. doi:10.1016/J.CEJ.2014.07.109.
- Tavakoli, O. and Yoshida*, H. (2005) "Effective Recovery of Harmful Metal Ions from Squid Wastes Using Subcritical and Supercritical Water Treatments," *Environmental Science and Technology*, 39(7), pp. 2357–2363. doi:10.1021/ES030713S.
- Tavakoli, O. and Yoshida, H. (2006) "Conversion of scallop viscera wastes to valuable compounds using sub-critical water," *Green Chemistry*, 8(1), pp. 100–106. doi:10.1039/B507441J.
- Timofeev, K.L. *et al.* (2017) "Sorption technology of indium extraction from zinc production solutions," *Izvestiya Vuzov. Tsvetnaya Metallurgiya (Izvestiya. Non-Ferrous Metallurgy)*, 0(2), pp. 43–50. doi:10.17073/0021-3438-2017-2-43-50.
- Tóth, J. (1994) "Thermodynamical Correctness of Gas/Solid Adsorption Isotherm Equations," *Journal of Colloid and Interface Science*, 163(2), pp. 299–302. doi:10.1006/JCIS.1994.1107.
- Understand and fix common STL file errors / Hubs* (no date). Available at: <https://www.hubs.com/knowledge-base/fixing-most-common-stl-file-errors/> (Accessed: August 26, 2021).
- USDI, U. and (2011) *USGS Mineral Commodity Summaries 2011*.
- USGS (2017) *Indium-in: USGS Mineral Commodity Summaries*.
- USGS (no date) *Historical Statistics for Mineral and Material Commodities in United states*.
- V, S., JN, H. and E, G. (2015) "Leaching capacity of metals-metalloids and recovery of valuable materials from waste LCDs," *Waste management (New York, N.Y.)*, 45, pp. 314–324. doi:10.1016/J.WASMAN.2015.05.025.
- Virolainen, S., Ibane, D. and Paatero, E. (2011) "Recovery of indium from indium tin oxide by solvent extraction," *Hydrometallurgy*, 107(1–2), pp. 56–61. doi:10.1016/J.HYDROMET.2011.01.005.
- Wang, F. *et al.* (2007) "Laser fabrication of Ti₆Al₄V/TiC composites using simultaneous powder and wire feed," *Materials Science and Engineering: A*, 445–446, pp. 461–466. doi:10.1016/J.MSEA.2006.09.093.
- Wang, F.Y., Wang, H. and Ma, J.W. (2010) "Adsorption of cadmium (II) ions from aqueous solution by a new low-cost adsorbent-Bamboo charcoal," *Journal of Hazardous Materials*, 177(1–3), pp. 300–306. doi:10.1016/J.JHAZMAT.2009.12.032.
- X, C. *et al.* (1993) "Synthesis of poly(acrylamidrazone-hydrazide) chelating fiber and application of enrichment-separation for traces of indium, tin, chromium, vanadium and

- titanium from solution samples,” *Talanta*, 40(4), pp. 527–532. doi:10.1016/0039-9140(93)80012-G.
- XIONG, C. and YAO, C. (2008a) “Sorption behavior of iminodiacetic acid resin for indium,” *Rare Metals*, 27(2), pp. 153–157. doi:10.1016/S1001-0521(08)60106-0.
- XIONG, C. and YAO, C. (2008b) “Sorption behavior of iminodiacetic acid resin for indium,” *Rare Metals*, 27(2), pp. 153–157. doi:10.1016/S1001-0521(08)60106-0.
- Xu, Z., Cai, J. and Pan, B. (2013) “Mathematically modeling fixed-bed adsorption in aqueous systems,” *Journal of Zhejiang University SCIENCE A* 2013 14:3, 14(3), pp. 155–176. doi:10.1631/JZUS.A1300029.
- Yakout, S.M. and Elsherif, E. (2010) “Batch kinetics, isotherm and thermodynamic studies of adsorption of strontium from aqueous solutions onto low cost rice-straw based carbons,” *India Carbon-Sci. Tech*, 1, pp. 144–153.
- Yang, J. *et al.* (2016) “Recovery of indium and yttrium from Flat Panel Display waste using solvent extraction,” *Separation and Purification Technology*, 166, pp. 117–124. doi:10.1016/J.SEPPUR.2016.04.021.
- Yang, J., Retegan, T. and Ekberg, C. (2013) “Indium recovery from discarded LCD panel glass by solvent extraction,” *Hydrometallurgy*, 137, pp. 68–77. doi:10.1016/J.HYDROMET.2013.05.008.
- Yoshida, H. *et al.* (2014) “Recovery of indium from TFT and CF glasses in LCD panel wastes using sub-critical water,” *Solar Energy Materials and Solar Cells*, 125, pp. 14–19. doi:10.1016/J.SOLMAT.2014.02.009.
- Yoshida, H. *et al.* (2015) “Recovery of indium from TFT and CF glasses of LCD wastes using NaOH-enhanced sub-critical water,” *The Journal of Supercritical Fluids*, 104, pp. 40–48. doi:10.1016/J.SUPFLU.2015.05.016.
- Yuan, Y. *et al.* (2010) “Synthesis of coated solvent impregnated resin for the adsorption of indium (III),” *Hydrometallurgy*, 101(3–4), pp. 148–155. doi:10.1016/J.HYDROMET.2009.12.010.
- Yuchi, A. *et al.* (1992) “Adsorption Mechanism of Trivalent Metal Ions on Chelating Resins Containing Iminodiacetic Acid Groups with Reference to Selectivity,” *Bull. Chem. Soc. Jpn*, 211(1), pp. 2941–2944.
- Z, A. and G, D. (2003) “A comparative study on the biosorption characteristics of some yeasts for Remazol Blue reactive dye,” *Chemosphere*, 50(8), pp. 1075–1083. doi:10.1016/S0045-6535(02)00623-9.
- Zhang, L. and Xu, Z. (2016) “A review of current progress of recycling technologies for metals from waste electrical and electronic equipment,” *Journal of Cleaner Production*, 127, pp. 19–36. doi:10.1016/J.JCLEPRO.2016.04.004.
- Zhang, Y. *et al.* (2010) “Effect of mechanical activation on the kinetics of extracting indium from indium-bearing zinc ferrite,” *Hydrometallurgy*, 102(1–4), pp. 95–100. doi:10.1016/J.HYDROMET.2010.02.003.

Zhang, Y. *et al.* (2017) “Separation of indium from lead smelting hazardous dust via leaching and solvent extraction,” *Journal of Environmental Chemical Engineering*, 5(3), pp. 2182–2188. doi:10.1016/J.JECE.2017.04.034.

ZHU, G. *et al.* (2007) “Recovering indium with sulfating roasting from copper-smelting ash,” *Rare Metals*, 26(5), pp. 488–491. doi:10.1016/S1001-0521(07)60250-2.